学位論文

Anatomical and functional studies on neural circuitry for nociception in *Drosophila* larvae

（ショウジョウバエ幼虫における侵害受容感覚を担う

神経回路の構造・機能的研究 ）

平成 29 年度 7 月博士（理学）申請

東京大学大学院理学系研究科

生物科学専攻

吉野 次郎

Contents

Abbreviations

- **C4da neurons** Class IV dendritic arborization neurons
- **mCSI** medial clusters of C4da second order interneuron
- **GRASP** GFP reconstitution across synaptic partners
- **VNC** Ventral nerve cord
- **ChR2** Channelrhodopsin-2
- **ATR** all-trans retinal
- **ReaChR** Red-activatable channelrhodopsin
- **TNT** Tetanus neurotoxin light chain
- **SNa** Segmental nerve a

Abstract

Animals possess the ability to detect and respond to various information from their environment. In particular, the ability to detect and avoid harmful stimuli, called nociception, is one of the most important factors for survival. How an animal transforms noxious stimuli into behaviors is largely unknown. Both in vertebrates and invertebrates, noxious stimuli are detected by specialized neurons and relayed to the central nervous system. The larvae of the fruit fly, *Drosophila melanogaster*, detect noxious stimuli by a special class of sensory neurons called C4da neurons, which tile their body wall. Behaviors such as cork-screw like rolling are triggered as a response to noxious stimuli. Various studies have uncovered the receptors essential for detection of noxious stimuli. However, the circuit mechanisms how the detected noxious information is transformed into behavior still remain elusive. To uncover the neural circuitry underlying nociceptive behavior, it is important to identify neurons that directly receive nociceptive signals from C4da sensory neurons.

In the present doctoral dissertation, I first identified neurons that directly receive nociceptive signals from C4da sensory neurons. By screening thousands of GAL4 expressing lines, I found neurons that are located in the projection areas of the C4da neurons in the ventral nerve cord (VNC), a structure analogous to the spinal cord of vertebrates. These neurons are segmentally arrayed in the abdominal segments A1-A7 of the VNC. I designated these neurons as medial clusters of C4da second order interneurons (mCSIs). To examine whether mCSIs receive monosynaptic inputs from C4da neurons, I performed GFP reconstitution across synaptic partner (GRASP) analysis. GRASP analysis indicated mCSIs are in close proximity to C4da neurons. Furthermore, calcium imaging revealed that mCSIs are functional downstream of C4da neurons. I imaged the calcium level of mCSIs and found

that it was significantly elevated upon the activation of C4da neurons. Collectively, these data suggest that mCSIs are directly connected to C4da and receive nociceptive information from C4da neurons.

Next, I performed behavioral analysis to test the involvement of mCSIs in nociceptive behavior. Direct activation of mCSIs by optogenetics triggered rolling behavior in all larvae tested, suggesting that activation of mCSIs is sufficient to trigger rolling. Silencing of mCSIs activity by blocking synaptic transmission significantly reduced the probability of rolling behavior, thus indicating that mCSIs are necessary to trigger rolling behavior. These data indicate mCSIs are necessary and sufficient for rolling behavior.

Finally, I attempted to identify the downstream neurons of mCSIs. By expressing GFP and dendrite marker simultaneously, I visualized the axonal projections of mCSIs. mCSI axons seemed to project to the dorsal region of the VNC, where dendrites of motor neurons are highly elaborated. Considering the possibility that mCSIs send output to motor neurons, I checked the axonal projection patterns of mCSI and motor neurons simultaneously. I found a close apposition between mCSI axonal terminals and one type of the motor neurons, SNa motor neurons, which project to transverse muscles in the body wall. Calcium levels of SNa motor neurons were elevated upon the activation of mCSIs. Silencing of SNa motor neurons significantly reduced the probability of C4da/mCSI-evoked rolling behavior without affecting basal crawling behavior. These data imply mCSIs send output to SNa motor neurons to trigger rolling behavior.

In summary, by combining anatomical, physiological, behavioral analysis, I found neural circuitry that evokes nociceptive rolling behavior in *Drosophila* larvae. This finding provides an entry point to understanding how nociceptive behaviors are controlled in

Drosophila larvae.

Introduction

Overview

Organisms possess the ability to detect noxious stimuli that could potentially cause tissue damage (Loeser and Treede, 2008). Such ability, defined as nociception, benefits animals by increasing their survival rate. In humans, patients suffering from channelopathies that impair the ability to detect noxious stimuli have very high rates of early mortality (Bennett and Woods, 2014). How an animal detects such stimuli and how response behaviors are evoked is of great interest in terms of both clinical importance and basic neuroscience.

Nociception in vertebrates

In vertebrates, intense thermal, mechanical, or chemical stimuli are detected by a subpopulation of peripheral nerve fibers, called nociceptors (Basbaum and Jessell., 2000). The cell bodies of nociceptors are located in the dorsal root ganglia and they have both peripheral and central branches that innervate either their target tissue or the spinal cord, respectively (Figure 1A). Nociceptors are divided into two major classes (Dubin and Patapoutian, 2010). The first includes thinly myelinated Aδ axons which conduct action potentials at the speed of 5 to 30 m/s. The second includes unmyelinated C axons that conduct more slowly, at the speed of less than 1 m/s.

The action potential in the nociceptors can either be relayed to the reflex arc in the spinal cord to provoke escape behavior (Flexion reflex, Figure 1A) or travel via spinal cord interneurons to higher order processing centers in the brain (Figure 1B). Previous studies have uncovered receptors for the detection of various nociceptive stimuli (Caterina et al., 1997; Bautista et al., 2007). However, relatively little is known about the mechanisms that control the behaviors evoked by noxious stimuli at the circuit level due to their neural

complexity or lack of genetic tools to investigate them.

Drosophila larvae, as a model system for nociception

The larvae of fruit fly, *Drosophila melanogaster,* has emerged as a good model to overcome underlying problems in vertebrate. The relatively small size of its nervous system (~10,000 neurons) is amenable to circuit identification. Powerful genetic tools enable the identification and structural/functional studies of neurons. The receptor genes expressed in vertebrate nociceptor exists in *Drosophila,* implying conserved molecular mechanism for nociception. The importance of nociception for animal's survival implies that nociception involves behavioral response and its underlying circuit mechanisms conserved across animals (Walters., 1994; Walters and Moroz., 2009; Woolf and Walters., 1991). An additional advantage is short life cycle in *Drosophila* about two weeks (Figure 2). After the egg is fertilized, the embryo hatches in ~24 hours. The larva undergoes successive molts to become the first, second and third instar larva. Late third instar larvae crawl out of the food to become the pupae. After several days, the adult flies eclose from the puparium. This short life cycle makes it possible to generate and study numerous transgenic lines within a short time period.

Nociceptive behavior of *Drosophila* larvae

Drosophila larvae show defensive behaviors in response to harsh mechanical stimuli, noxious heat and attacks from predators. For examples, larvae exhibit cork-screw like rolling behavior when 42℃ heat probe or 45 mN mechanical stimuli are applied to their body

wall (Tracey et al., 2003). They also exhibit the rolling behavior when attacked by a parasitoid wasp, a known predator that injects eggs into *Drosophila* larvae by using their ovipositor (Hwang et al., 2007; Robertson et al., 2013).

Organization of the sensory system in *Drosophila* larvae

Drosophila larval nervous system is composed of peripheral and central nervous systems (PNS and CNS). In PNS, many sensory neurons are located on their body wall (Figure 3A). They are classified according to their morphology and innervating organs (Bodmer and Jan, 1987)(Figure 3B). These neurons detect different modalities of external stimuli or internal somatosensation. For instance, neurons in chordotonal organ detect vibrations (Zhang et al., 2013) and are involved in proprioception (Caldwell et al., 2003). Among these sensory neurons, a class of dendritic arborization (da) neurons are especially important for larval nociception. The da neurons are classified into four groups: Class Ⅰ, ClassⅡ, ClassⅢ and ClassⅣ in the order of increasing complexity of dendritic branches (Gruber et al., 2002). Besides their morphological differences, these four classes of da neurons can be distinguished by their functional properties as well. Class Ⅰ neurons are involved in locomotion and also function as proprioceptors (Cheng et al., 2010) . The functions of ClassⅡ neurons are not well understood so far, although their involvement in touch sensation has been postulated (Tsubouchi et al., 2012). ClassⅢ neurons act as touch sensors (Tsubouchi et al., 2012; Yan et al., 2013). As ClassⅣ da (C4da) neurons are necessary and sufficient to induce larval escape behavior, this type of neurons are considered as primary detectors for nociceptive stimuli. Three C4da neurons exist in each hemisegment (Figure 4A). C4da neurons elaborate highly branched dendritic trees and are activated by

noxious heat, harsh mechanical stimuli and noxious light such as blue or ultra violet, through distinct receptors (Im and Galko, 2012; Xiang et al., 2010), and considered as a counterpart for the vertebrate's nociceptors. The action potentials generated in the C4da neurons are relayed to the CNS where the axons occupy specific regions of the ventral nerve chord (VNC, Figure 4B).

C4da neuron, the primary detector of noxious stimuli

The C4da neurons elaborate highly branched dendritic trees that directly innervate the epidermis (Jan and Jan., 2010; Emoto., 2012; Kanamori et al., 2015; Grueber et al., 2002; Koike-Kumagai et al., 2009; Kanamori et al., 2013; Yasunaga et al., 2010; Han et al., 2012) and are required for larval nociception. In fact, silencing or ablation of C4da neurons largely eliminates larval responses to noxious stimuli (Hwang et al., 2007; Xiang et al., 2010; Robertson et al., 2013; Ohyama et al., 2015). Several studies identified molecules required for detection of nociceptive stimuli. *Pickpocket (ppk)*, an ion channel subunit of the Degenerin/Epithelial sodium channel (DEG/ENaC) is required for mechanical nociception, but dispensable for thermal nociception and expressed in C4da neurons (Zhong et al., 2010). Piezo is a mechanosensitive ion channel protein in mammals (Coste et al., 2010). *Drosophila* homolog of mammal's piezo, DmPiezo in C4da neurons is also required for mechanical nociception, but not for the thermal nociception (Kim et al., 2012). DmPiezo, has a role in generating currents in response to mechanical stimuli although they do not have extensive sequence conservation (24% identity). A member of transient receptor potential (TRP) ion channel family, called painless, is required for both mechanical and thermal nociception (Tracey et al., 2003). Although whether painless gene is indeed required for the nociceptive

behavior in C4 da neurons is unclear, at least the protein of painless is known to exist in multidendritic neurons (Tracey et al., 2003). Another member of TRP channel, TRPA1 is required for thermal nociception and light avoidance (Neely et al., 2011; Xiang et al., 2010). Thermal nociceptive behavior is impaired by RNAi-mediated *TrpA1* knock down in multidendritic neurons, suggesting this gene in multidendritic neurons is required for thermal nociception. Besides thermal nociception, TRPA1 in C4da neurons plays a role in avoidance behavior. RNAi-mediated *TrpA1* knock down in C4da eliminates the firing response in C4da and the avoidance behavior in response to high intensity blue or ultraviolet light.

Furthermore, optogenetic activation of C4da neurons is sufficient to provoke corkscrew-like rolling behavior similar to what is observed when larvae receive noxious stimuli such as high temperature and harsh mechanical stimulation or attack from predator (Hwang et al., 2007; Xiang et al., 2010; Ohyama et al., 2015)(Figure 5). These evidence strongly suggest that C4da neurons are necessary and sufficient for the nociceptive behavior and that these neurons are the primary nociceptive sensory neurons in *Drosophila* larvae.

Neural circuit for nociceptive behavior

Whereas the receptors and the regulatory mechanisms of C4da activation in response to a variety of noxious stimuli have been well studied (Adams et al., 1998; Tracey et al., 2003; Neely et al., 2011; Kim et al., 2012; Guo et al., 2014; Honjo et al., 2016; Mauthner et al., 2014; Babcock et al., 2009; Babcock et al., 2011; Im et al., 2015; Terada et al., 2016), how C4da activation triggers the escape behavior in the circuit level remains elusive. Previous study uncovered a type of C4da second order neuron designated as Basin, which promotes rolling behavior by integrating vibration detected by ch neurons and nociceptive

stimuli detected by C4da neurons (Ohyama et al., 2015). Four basins exist in each hemisegment of VNC, designated as Basin-1~4 respectively (Figure 6A). Basin-1 and Basin-2 receive inputs from ch neurons, Basin-2 and Basin-4 receive inputs from both ch neurons and C4da neurons. The excitation of Basins is relayed to another interneuron named A05q and A23g, and subsequently command-like interneuron Goro (Figure 6B). This neural circuit enhances probability of rolling behavior when nociceptive stimuli and vibration are simultaneously detected. However, inhibition of Basins or Goro neurons do not completely eliminate rolling behavior, it seems these Basin or Goro inhibition eliminate only enhanced probability of rolling behavior when nociceptive stimuli and vibration are detected, not the basal probability of rolling behavior induced by the activation of C4da alone. These data imply Basin-Goro pathway functions only in the multimodal nociceptive-vibration integration. Thus, there might be other neural circuits that can trigger or facilitate rolling in parallel with Basin-Goro pathway.

In this doctoral dissertation, I identified another type of C4da second order neuron designated as mCSI. mCSIs are segmentally located in A1-A7 segments of the ventral nerve cord (VNC). GRASP and calcium imaging analysis revealed mCSIs are structurally and functionally downstream of C4da neurons. Activation of mCSIs is sufficient to trigger rolling. In addition, mCSIs are required for the normal level of rolling in response to C4da activation. mCSIs act in parallel with the Basin-Goro pathway, as the silencing of Goro does not affect mCSI-induced rolling behavior. Finally I provided anatomical and calcium imaging evidence that suggest mCSIs may send output to SNa motor neurons.

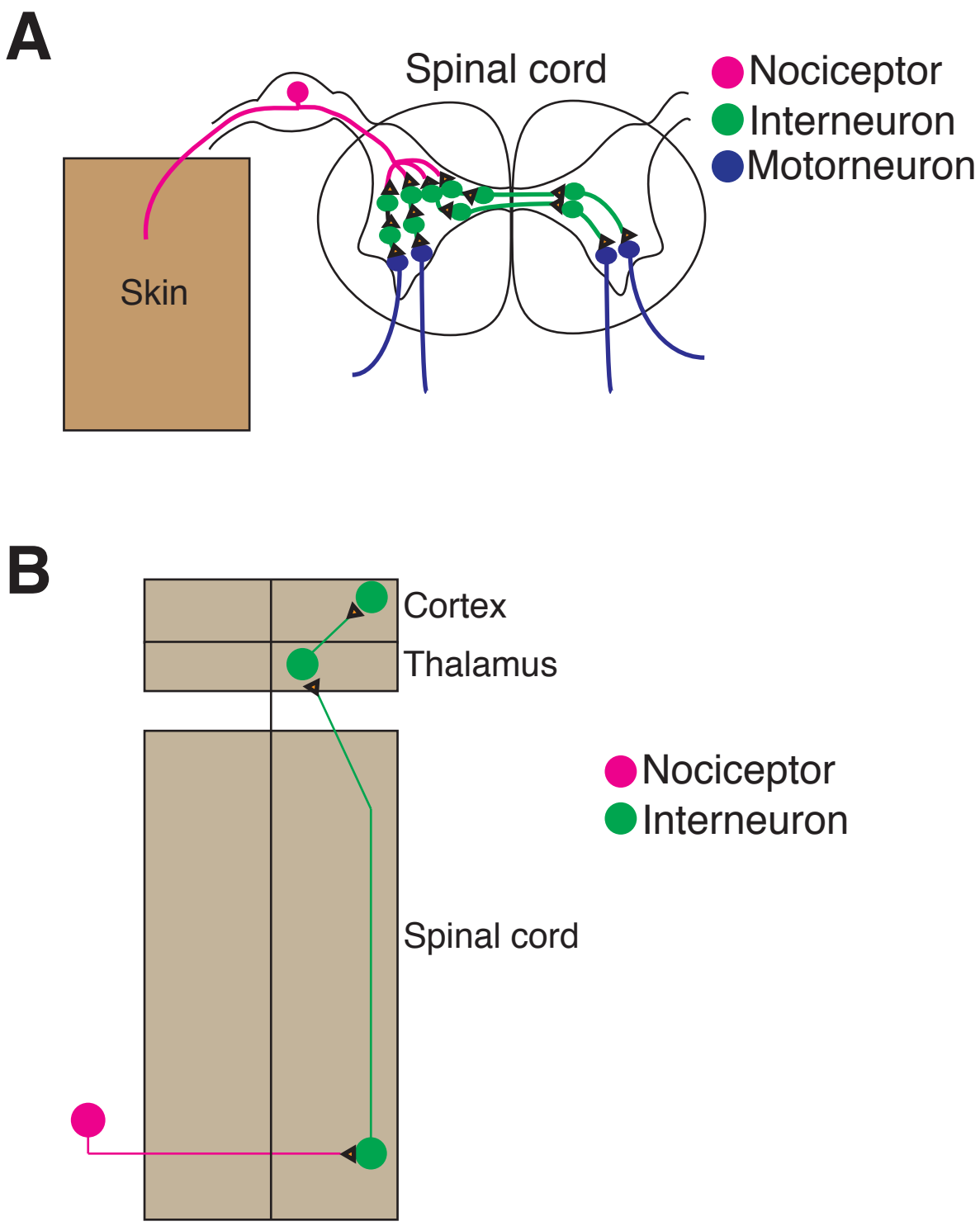

Figure 1. Schematic representation of vertebrate neural circuits for nociception
(A) Schematic representation of the reflex circuit for nociception. The action potentials generated by the nociceptors located in the dorsal root ganglia are relayed to motor neurons via interneurons in the spinal cord. The firing of motor neurons leads to escape behavior (Flexion reflex).
(B) Schematic representation of ascending neural circuit for nociception. The action potentials generated by the nociceptors also relayed to another interneuron and ascend to the thalamus and subsequently to the cortex.

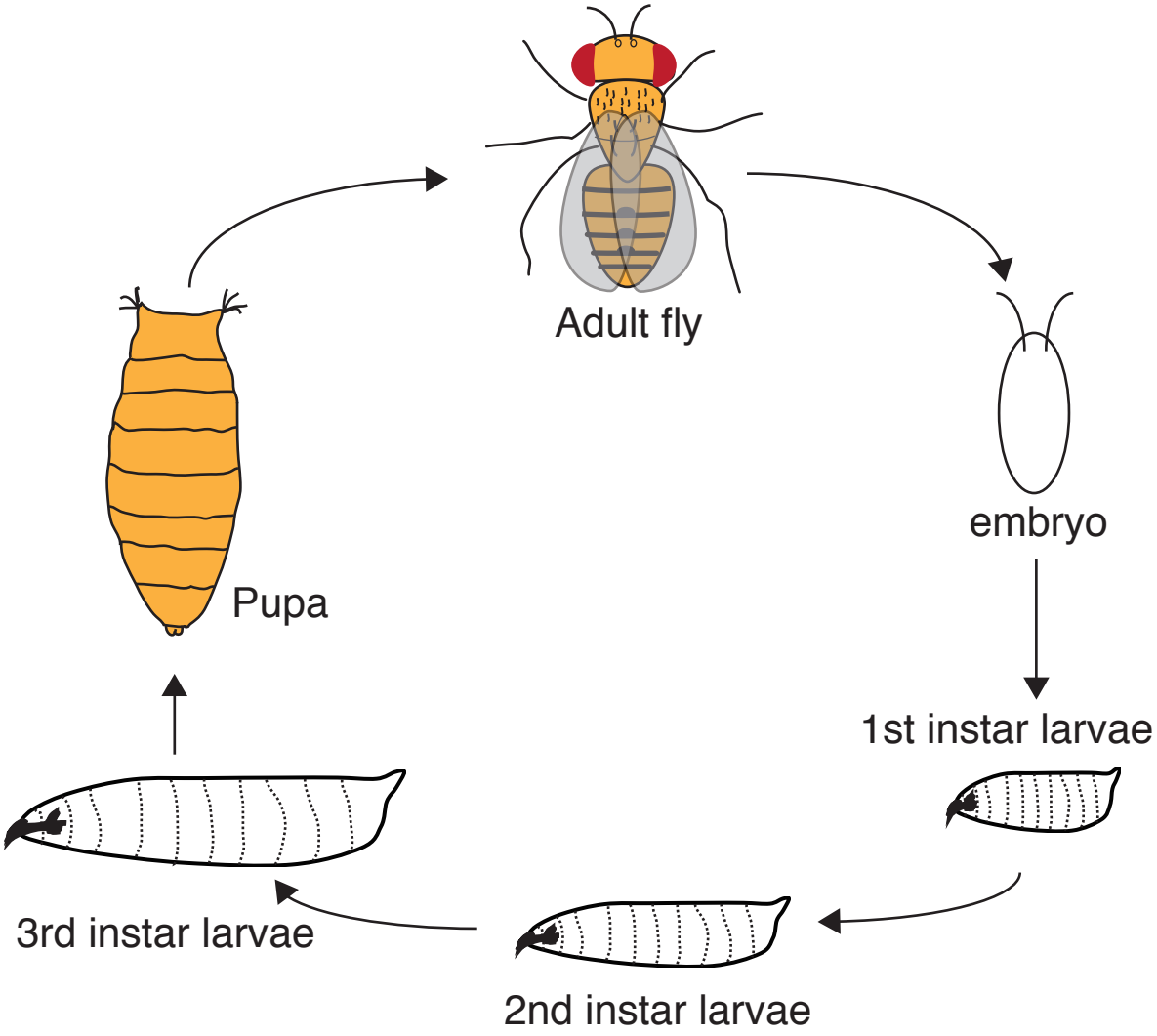

Figure 2. Life cycle of the model organism fruit fly, *Drosophila melanogaster*

At 25°C, embryo of fruit fly develops into adult via three larval stages (4-5 days) and a pupal stage (4-5 days).

A

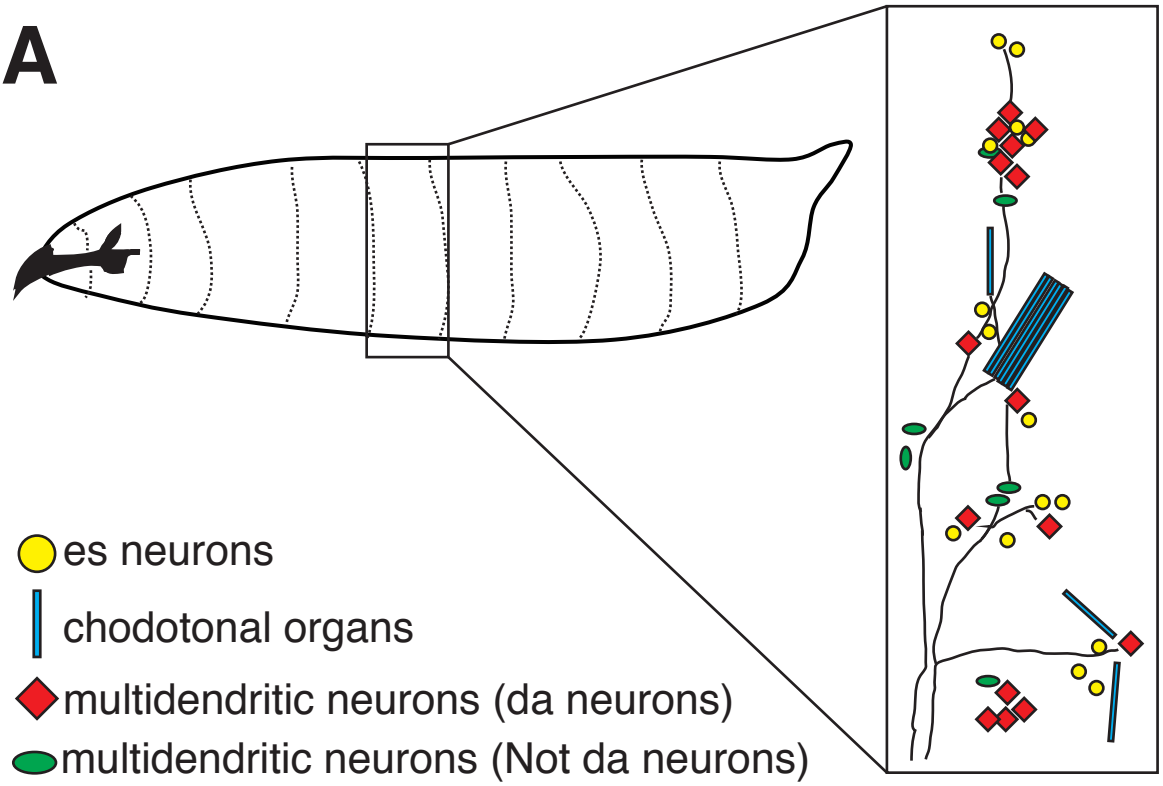

B

			Multidendritic neurons		
	es neurons	ch neurons	da neurons	bd neurons	td neurons
dendrite morphology	single dendrite	single dendrite	multiple dendrites	bipolar dendrites	multiple dendrites
innervating targets	external sensory organs	chodotonal organs	free nerve ending	free nerve ending	tracheal branches

Figure 3. *Drosophila* larval sensory neurons

(A) Schematic representation of larval sensory neurons on the body wall. es neurons (yellow circles) , chordotonal organs (blue rectangles), da neurons (red diamonds), other multidendritic neurons (green circles).

(B) Table for classification of each sensory neurons. These neurons are classified according to their dendrite morphology and innervating targets.

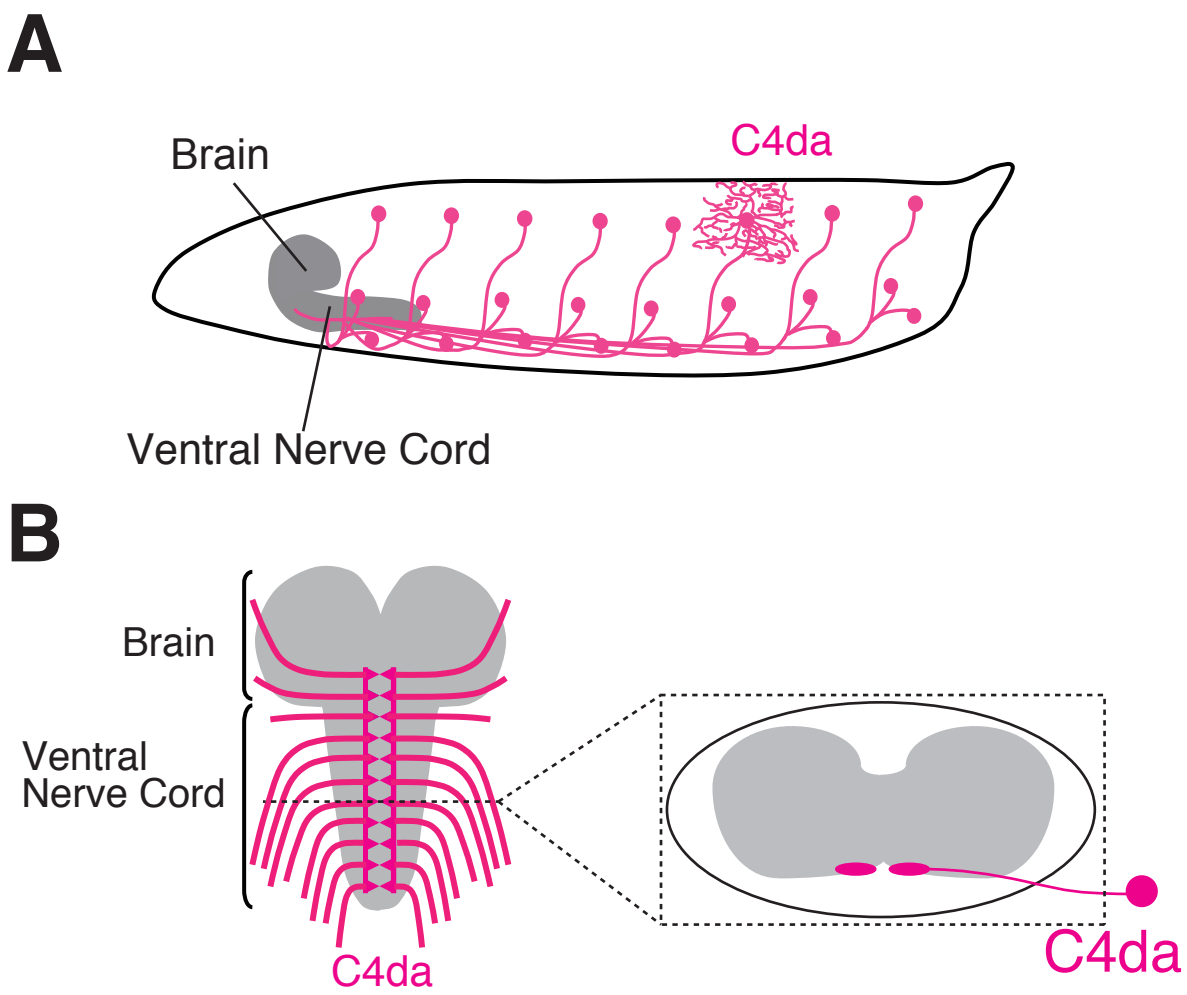

Figure 4. Schematic organization of C4da neurons

(A) Schematic lateral view of dendrite arborization and axonal projections of C4da neurons in the third instar larva.

(B) Schematic ventral view of the axonal terminal projections of C4da neurons in the VNC (left) and coronal section of dashed line (right).

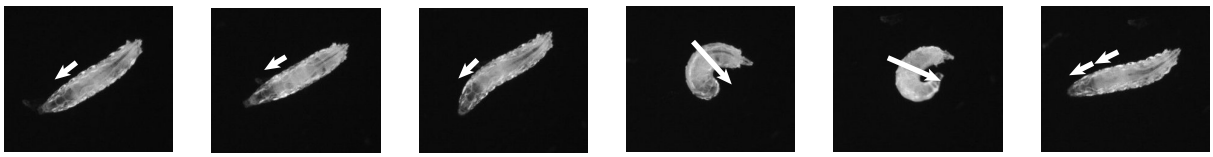

Figure 5. Optogenetic activation of C4da neurons induces rolling behavior

Each arrow indicates the direction of larval movement. The orange line represents optogenetic activation of C4da neurons. Upon optogenetic activation of C4da neurons, the larvae exibit corkscrew-like rolling behavior around the anterior/posterior axis.

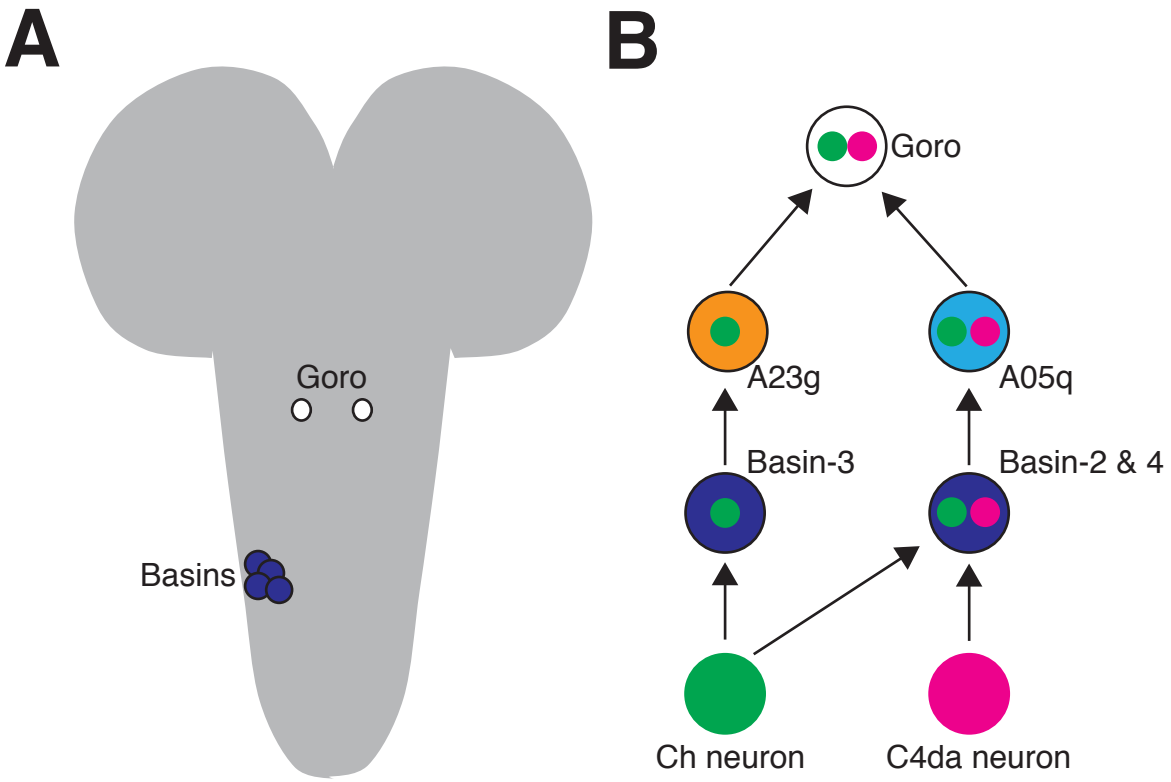

Figure 6. Neural circuit for multimodal integration, Basin-Goro pathway
(A) Soma position of Basins (Blue circles) at A7 segment and Goro (white circles) respectively. Only one hemi-segment of Basins are shown in this scheme.
(B) Circuit diagram of Basin-Goro pathway for multimodal integration. Vibration and nociceptive information are converged at Basin-2 and 4 and Goro (multilevel convergence).

Materials and Methods

Fly stocks and transgenic flies

The following list summarizes the *Drosophila* strains used in this study.

Experimental Models: Organisms/Strains		
Drosophila, w^{1118}	Bloomington	Stk#3605
Drosophila, UAS-TNT	Bloomington	Stk#28838
Drosophila, R94B10-GAL4	Bloomington	Stk#41325
Drosophila, R52F05-GAL4	Bloomington	Stk#48192
Drosophila, R69F06-GAL4	Bloomington	Stk#39497
Drosophila, UAS-mCD8GFP	Bloomington	Stk#32186
Drosophila, ppk-CD4-tdTomato	Bloomington	Stk#35845
Drosophila, UAS-ReaChR	Bloomington	Stk#53749
Drosophila, UAS-GCaMP6m	Bloomington	Stk#42748
Drosophila, TRPA1QF	Bloomington	Stk#36345
Drosophila, QUAS-ChR2[H134R]		(Kanamori et al., 2015)
Drosophila, yw,LexAop-mCD8GFP,UAS-mCD8RFP	Bloomington	Stk#32229
Drosophila, LexAop-GAL80	Bloomington	Stk#32214
Drosophila, LexAop-ReaChR	Bloomington	Stk#53746
Drosophila, UAS-DenMark	Bloomington	Stk#33062
Drosophila, UAS-nsyb-spGFP$_{1-10}$, LexAop-CD4-spGFP$_{11}$	Bloomington	Stk#64314
Drosophila, UAS-Dα7::GFP	Bloomington	Stk#39692
Drosophila, LexAop-Brp (short)::mCherry	Gift from Peter Soba	N/A
Drosophila, R27H06-LexA	Bloomington	Stk#54751
Drosophila, hs-flp	Bloomington	Stk#6
Drosophila, NP4099	DGRC	Stk#104601
Drosophila, UAS>CD2>CD8::GFP	Gift from Kristin Scott	N/A
Drosophila, R72F11-LexA	Gift from Gerald Rubin	N/A
Drosophila, ppk-LexA	This study	N/A
Drosophila, R94B10-LexA	This study	N/A
Drosophila, BarH1-GAL4	Gift from Iris Salecker (Sato et al., 1999)	
Drosophila, LexAop-CD2RFP	Gift from Tzumin Lee	
Drosophila, Tsh-GAL80	Gift from Gero Miesenböck (Clyne et al., 2008)	
Drosophila, LexAop-CD4-spGFP$_{11}$-tdTomato	Gift from Peter Soba	
Drosophila, UAS-CD4-spGFP$_{1-10}$	Gift from Kristin Scott	

Drosophila third instar wandering larvae of mixed sexes were used in all experiments except for dual labeling of SNa motor neurons and mCSIs. In the case of the dual labeling, I used female larvae to express transgenes from different X chromosomes. Larvae were raised on standard medium at 25℃ unless otherwise specified. Fly stocks carrying *w^{1118}*, *UAS-TNT*, *R94B10-GAL4*, *R52F05-GAL4*, *R69F06-GAL4*, *UAS-mCD8GFP*, *ppk-CD4-tdTomato, UAS-ReaChR, UAS-GCaMP6m, TRPA1QF, LexAop-mCD8GFP, UAS-*

mCD8RFP, LexAop-GAL80, LexAop-ReaChR, UAS-DenMark, UAS-nsyb-spGFP$_{1-10}$, LexAop-CD4-spGFP$_{11}$ and *hs-flp* were obtained from the Bloomington *Drosophila* Stock Center. *NP-4099* was obtained from the *Drosophila* Genetic Resource Center. *UAS>CD2>mCD8GFP* and UAS-CD4-spGFP$_{1-10}$ was provided by K. Scott (University of California); *LexAop-Brp-short-mCherry* and *LexAop-CD4-spGFP$_{11}$-tdTomato* by P. Soba (Center for Molecular Neurobiology, Hamburg); *LexAop-CD2RFP* by T. Lee (Janelia Research Campus); *Tsh-GAL80* by Gero Miesenböck (University of Oxford); *BarH1-GAL4* by I. Salecker (The Francis Crick Institute) and *R72F11-LexA* by G. Rubin (Janelia Research Campus). *QUAS-ChR2[H134R]* was generated by T. Kanamori (Kanamori et al., 2015). *ppk-LexA* line was constructed by cloning *ppk* promoter region cut from ppk-hs-EGFP vector (Gruber et al., 2003) into pCR8/GW/TOPO (Thermo Fisher Scientific) and subsequently exchanged to pBPnlsLexA::p65Uw according to previously described method (Pfeiffer et al., 2010). *R94B10-LexA* was generated by cloning the *R94B10* sequence present in PCR8/GW/TOPO (gift from G. Rubin) into pBPnlsLexA::p65Uw according to the same method as *ppk-LexA*.

GAL4/UAS system

The GAL4/UAS system is a binary expression system consisting of two main components: the yeast GAL4 transcriptional activator expressed in a specific spatiotemporal pattern and a transgene under the control of an Upstream Activation Sequence (UAS) promoter. This promoter is largely silent in the absence of GAL4 (Brand and Perrimon., 1993) (Figure 7A). GAL4 expression can be driven by defined enhancer elements or or random insertion of *GAL4* sequence into the genome such that it reports the *cis*-regulatory

architecture of the insertion location. Additionally, the GAL4/UAS system is repressible by the GAL80 protein which bind directly to GAL4 (Ma and Ptashne., 1987) (Figure 7B). LexA/LexA operator (LexAop) and QF/QUAS systems are generated as the second and third independent binary expression systems for *Drosophila* (Lai and Lee., 2006; Potter et al., 2010). LexA and QF bind to and activate *LexAop* and *QUAS*, respectively, allowing GAL4 independent target effector gene expression (Figure 7A).

Optogenetics

Optogenetics is a technique that involves the use of light to control cells, typically neurons, by expressing light-sensitive ion channels. In this study, light-gated cation channel channelrhodopsin2 or its variant were used. Channelrhodpsin2 (ChR2) is derived from the unicellular green alga *Chlamydomonas reinhardtii* (Nagel et al., 2003). ChR2 is gated by 470 nm blue light and produces inward currents (Figure 8). ChR2 was found to confer millisecond-precision control of neuronal spiking when introduced into neurons (Boyden et al., 2005). Red-activatable ChR (ReaChR) is a variant of ChR which is gated by 670 nm red light and is used for the same purpose as ChR2 (Lin et al., 2013).

Immunostaining

Third-instar wandering larvae were dissected and fixed in 4% formaldehyde/PBS for 30 min at room temperature. After fixation, the samples were washed five times in PBS containing 0.1% triton X-100 (PBST) and blocked for two hours in PBST containing 5% normal goat serum (NGS) at room temperature. The samples were subsequently incubated at 4℃ overnight with primary antibody containing 5% NGS/PBST. The samples were washed 5

times by PBST and consequently incubated with the secondary antibody overnight. The stained samples were mounted in VECTASHIELD mounting medium (Vector Laboratories), and images were observed by confocal microscopy (Leica TCS SP8). The primary antibodies used in this study were: anti-GFP (3E6, Wako), anti-CD8 (RM2200; invitrogen), and anti-CD2 (OX-54; Serotec). Fluorescently conjugated secondary antibodies used were anti-mouse Cy2 (Jackson ImmunoResearch), anti-mouse Cy3 (Jackson ImmunoResearch), anti-rat Cy2 (Jackson ImmunoResearch).

The antibodies used in this study are summarized in the following list.

Antibodies		
Anti-GFP antibody produced in mouse 3E6	Wako	Cat#542-00771
Anti-CD8 antibody produced in rat Ly-2	Invitrogen	Cat#RM2200
Anti-CD2 OX-54 antibody produced in mouse OX-54	Serotec	Cat#MCA443R
Anti-mouse secondary antibody Cy2	Jackson ImmunoResearch	Cat#115-225-166
Anti-mouse secondary antibody Cy3	Jackson ImmunoResearch	Cat#115-165-166
Anti-rat secondary antibody Cy2	Jackson ImmunoResearch	Cat#112-225-167

Calcium Imaging

Third-instar larvae raised on the fly food containing 1 mM all-trans retinal (Sigma) were dissected in HL3.1 solution without Ca^{2+} (Feng et al., 2004). The larvae were dissected along the dorsal midline and pinned on a silicon dish (Silpot 184, Dow Corning Toray). The internal organs except for neural tissue were removed. The ventral nerve cord was imaged using an Olympus BX51WI, equipped with a spinning-disk conforcal unit Yokogawa CSU10 (Yokogawa) and an EM-CCD digital camera (Evolve, Photometrics). For activation of C4da neurons with the light gated ChR2, blue light was delivered by pE-100 (CoolLED). During the 2 sec activation of C4da neurons, images were not acquired to avoid the halation of the images.

For the quantification of GCaMP6m fluorescence intensity, Metamorph software

(https://www.moleculardevices.com/systems/metamorph-research-imaging) was used. ⊿F is calculated according to the fomula $\triangle F = (F-F_0)/F_0$. F_0 is the mean intensity of the last ten time points before the light delivery.

Single Cell Analysis

GFP-labeled clones were generated in flies using transgenes to flip-in GFP, as described previously (Wong et al., 2002)(Figure 9). Flies of the genotype *hsflp; R94B10-GAL4/UAS >CD2 >mCD8GFP* were allowed to lay eggs for 24 hours. After egg collection, the larvae were allowed to develop for 24 hours. The larvae were then treated with single heat shock for 15 or 30 minutes at 38℃. These larvae were allowed to develop into third-instar stage and subsequently the CNS were dissected out, fixed by 4%PFA/PBS solution and mounted in VECTASHIELD mounting medium (Vector Laboratories). Images were acquired by confocal microscopy (Leica TCS SP8).

Behavioral Analysis

Third-instar larvae were allowed to develop on the fly food containing 1 mM all-trans retinal (Sigma). Before the experiments, the larvae were separated from food and washed with deionized water. Five larvae were then placed at the center of the arena. The substrate of the behavioural experiments was 1% agarose S gel (Nippon gene) in a 10×10 cm square plastic plate. For optogenetic activation, we delivered light (617 nm, ~35 μW/mm^2) for 15 seconds. The larval behaviors were recorded with CCD-Camera (1500M-GE, THORLABS). Crawling speed was measured using MWT software (http://sourceforge.net/projects/mwt). Only the larvae tracked for more than 5 sec were used

for speed calculations. In addition, the data before the onset of light delivery was used in quantification of the speed and turning.

Statistical Methods

All statistical analyses were performed using MATLAB (http://www.mathworks.com/). Statistical significance was evaluated by Fisher extract test or Welch's *t*-test. Benjamini-Hochberg correction was used for multiple testing. In Figures 15D, 21E, 22D, 23C and 23D, Welch's *t*-test were used. In Figures 18, 19A, 19B, 20, 21B, 21C, 23A and 23B, Fisher exact test was used. In the case of calcium imaging (Figures 15D, 21E and 22D), n indicates the number of cells. In other cases, n indicates the number of animals. I did not use any methods to determine whether the assumptions of the statistical approach were satisfied.

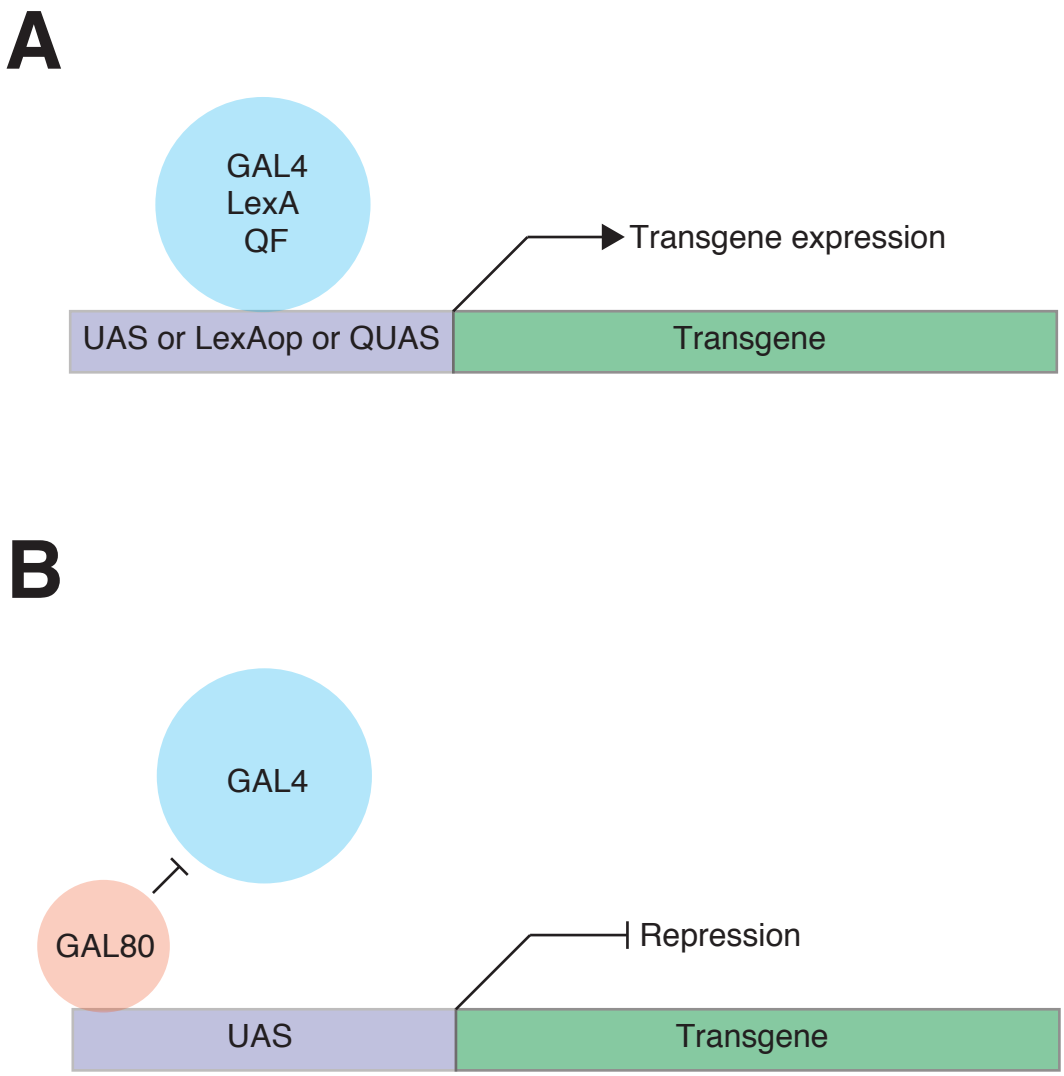

Figure 7. Binary expression systems in *Drosophila*

(A) Two-component expression sytems such as GAL4-UAS, LexA-LexAop or QF-QUAS consist of a transcriptional activator expressed in a spcific pattern and a transgene under the control of a promoter that is largely silent in the absence of the transcriptional activator.
(B) The GAL4-UAS system is repressible by the GAL80 protein, which binds to GAL4 and represses its transcriptional activity.

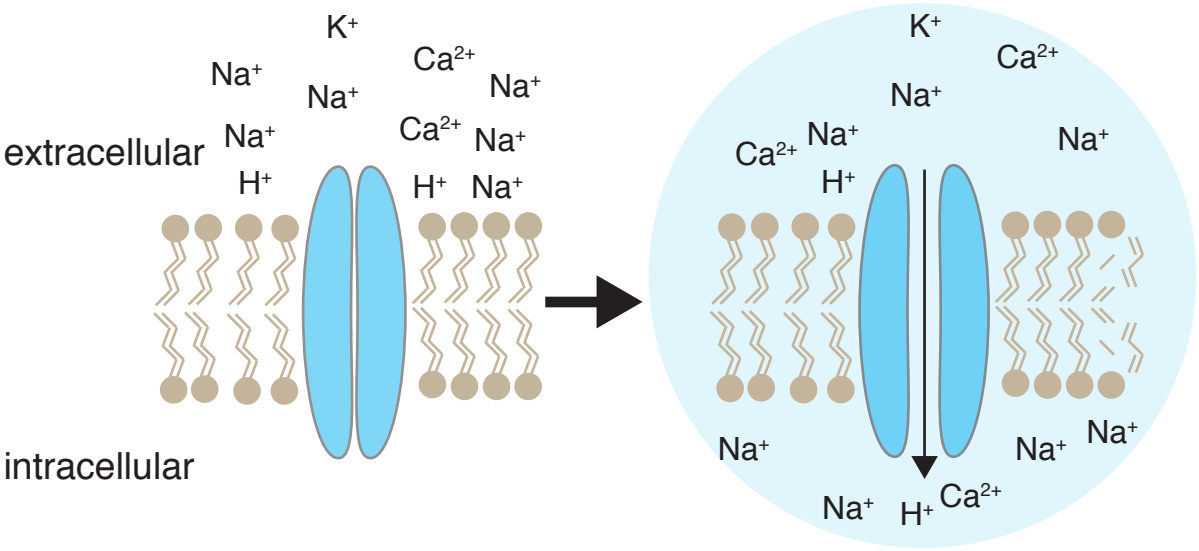

Figure 8. Schematic representation of channelrhodpsin-2

Channelrhodopsins are almost silent without blue light illumination. Channelrhodopsins passively conduct cations and depolarize neurons by opening its pore upon blue light illumination (right).

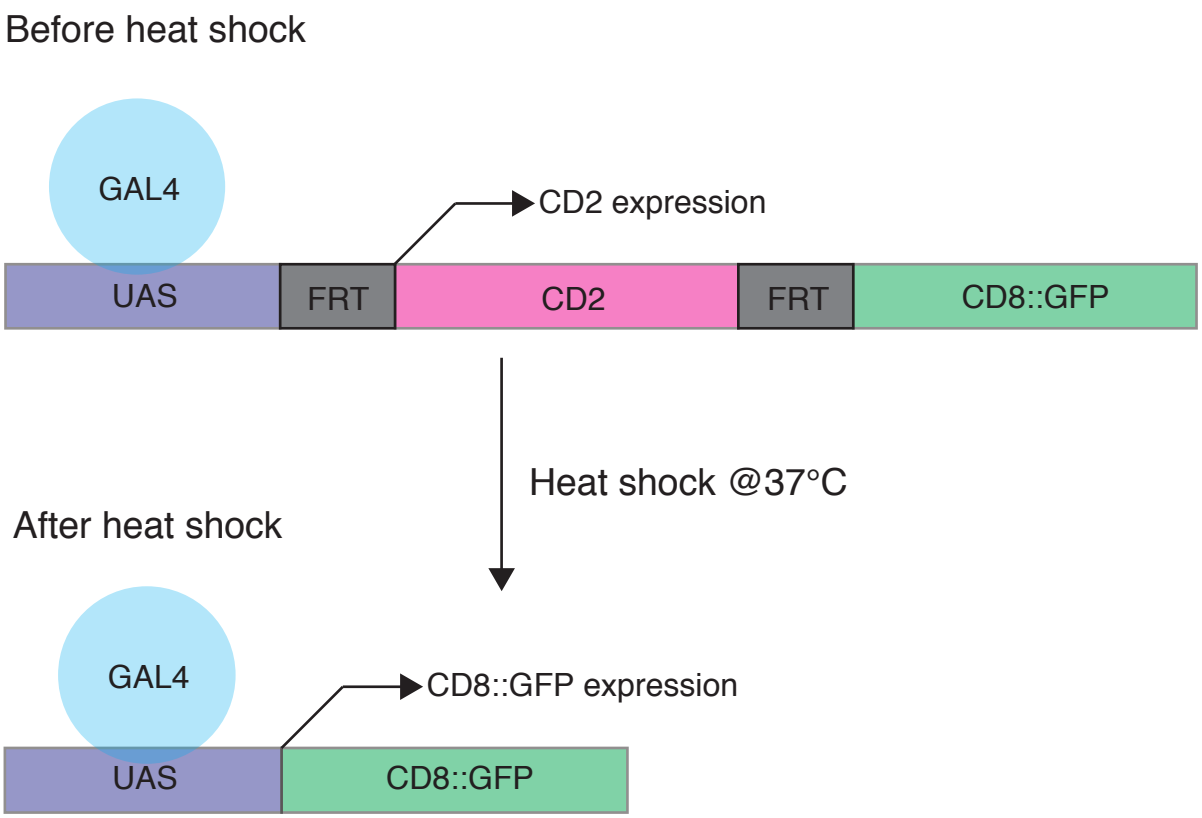

Figure 9. Heat shock mediated Flip-out system

Before heat shock, *CD2* is transcripted under the presence of GAL4. Upon heatshock, flipase, which is under the control of heat shock promoter, starts to be transcripted, subsequently recombines their target sequence FRT flancked locus. This occurs stochastically wihch enables to label neurons at single cell resolution.

Results

mCSIs are second-order neurons of C4da nociceptive sensory neurons

The C4da neurons have a unique axonal projection to a specific medial-ventral ladder-like pattern in the ventral nerve cord (VNC) (Figure 4B) (Grueber et al., 2007; Morikawa et al., 2011; Yang et al., 2014.) To identify second-order neurons to which C4da axons connect in the VNC, I screened ~1,000 Janelia GAL4 lines (Jenett et al., 2012). I found 2 independent lines, *R94B10-GAL4* and *R52F05-GAL4*, that drive GFP in neurons whose neurites overlap with the regions occupied by C4da axonal terminals (Figures 10A, 10B and 11). Although the two GAL4 lines drive GFP in different cell populations in the VNC as well as in the brain, they seemed to share a pair of neurons near C4da axon terminals in the abdominal segments A1‐7. To confirm that the two independent GAL4 lines labeled the same neurons in the VNC, I swapped the GAL4 enhancer element of the *R94B10-GAL4* with the *LexA* enhancer sequence and doubly labeled the neurons by both the GAL4/UAS and the LexA/LexAop binary expression systems (Venken et al., 2011). These dual-labeling experiments confirmed that the two GAL4 lines share only the segmentally arrayed neurons near the C4da axon terminals in each of abdominal segment A1-7 (Figure 12). I designated these neurons as mCSIs (medial clusters of C4da second-order interneurons).

To examine weather C4da axons might form contacts with mCSIs, I conducted GFP reconstitution across synapse partners (GRASP) analysis (Feinberg et al., 2008). When membrane-targeted version of the split GFP_{1-10} fragment and the split GFP_{11} fragment fused with td-Tomato were expressed in mCSIs and C4da neurons, respectively, reconstituted GFP signals were observed specifically in the region where C4da axon terminals innervated mCSI dendritic domains (Figure 13A). No significant GFP signal was detected in the same region when either of the split GFP fragment alone was expressed in mCSIs or C4da neurons

(Figures 13B and 13C), indicating the specificity of the GRASP signal. The contacts between C4da neurons and mCSIs are further confirmed by the following two experiments. First, I utilized the activity-dependent delivery of split-GFP tagged Synaptobrevin to the synaptic surface for GFP reconstitution across synapses (Syb-GRASP) (Macpherson et al., 2015). This resulted in the specific GFP signal along the entire C4da axon ladders (Figure 13D). Second, I expressed the presynaptic marker Brp-short-mCherry (Christiansen et al., 2011) in C4da neurons and the postsynaptic marker Dα7-GFP (Christiansen et al., 2011) in mCSIs, and found that C4da presynaptic zones are in apposition to mCSI postsynaptic area (Figure 14). These data suggest contacts between C4da axon terminals and mCSI dendrites.

Next, to examine whether mCSIs are functionally coupled to C4da neurons, I performed calcium (Ca^{2+}) imaging of mCSIs upon C4da activation. To that end, I expressed the blue light-activated cation channel Channelrhodopsin2 (ChR2) in C4da neurons and the Ca^{2+} sensor GCaMP6m in mCSIs (Figure 15A), and monitored mCSI Ca^{2+} response following C4da stimulation. Blue light stimulation of third instar larvae evoked a strong Ca^{2+} elevation in mCSIs (Figures 15B-15D; 363.92 ± 57.41 % elevation of $Fmax/F_0$ on average, n = 37). By contrast, Ca^{2+} levels were largely unchanged in larvae raised on media lacking all trans-retinal (ATR), the opsin essential for ChR2 activation (Figures 15B-15D: 24.35 ± 2.04 % elevation of $Fmax/F_0$ on average, n = 12). These evidence supports the idea that C4da activation evokes Ca^{2+} elevation in mCSIs. Taken together, my data show that mCSIs and C4da neurons are in close proximity and are functionally coupled, indicating that mCSIs are likely the second-order neurons of C4da nociceptive sensory neurons.

Single cell analysis of mCSIs

To characterize mCSIs at single cell resolution, I stochastically labeled single mCSI using the heat shock mediated flip-out system (Wong et al., 2002). Briefly, I used *R94B10-GAL4* to express the UAS-FRT-CD2-FRT-mCD8GFP cassette and labeled single mCSI with mCD8GFP using heat shock induced stochastic expression of flippase (FLP). As expected, mCSIs elaborate their neurites along the C4da axonal terminals (Figure 16A). In addition, mCSIs extend several neurites toward the dorsal neuropile region (Figures 16B and 16A). To delineate axonal and dendritic domains of mCSIs, I simultaneously expressed mCD8GFP and DenMark, a fusion protein of mouse ICAM5/Telencephalin and mCherry (Nicolaï et al., 2010), in mCSIs. I found that mCSIs elaborate dendrites along C4da axons while extending axons toward the dorsal neuropile region (Figure 16B).

I next examined the segmental organization of the Flp-out mCSI clones in the VNC. Previous studies showed that C4da axons extend both ipsilateral and contralateral branches to the innervating segments (Grueber et al., 2007; Morikawa et al., 2011). In contrast, mCSIs predominantly project ipsilateral dendritic branches (Figures 16A and 17). In addition, mCSIs typically extend dendrites to several anterior neighboring segments (Figure 17).

mCSI activation is necessary and sufficient for C4da-induced escape behavior

Given that mCSIs are innervated by C4da sensory neurons that receive nociceptive stimuli and evoke escape behaviors in larvae, I next wanted to examine whether mCSIs are involved in control of nociceptive behavior. To examine this possibility, I expressed the red-shifted variant of channelrhodopsin ReaChR (Lin et al., 2013) in mCSIs, optically stimulated these neurons, and monitored larval behavioral responses. Red light (610 nm) application to larvae harboring *R94B10-GAL4* and *UAS-ReaChR* evoked robust rolling behavior in all larvae tested (Figure 18). Similarly, 100 % of larvae harboring *R52F05-GAL4* and *UAS-ReaChR* showed rolling behavior in response to red light application (Figure 18). No rolling behavior was observed in larvae harboring either *GAL4* or *UAS-ReaChR* alone following red light exposure (Figure 18). Thus, activation of mCSI is sufficient to trigger nociceptive escape behavior, consistent with mCSI functioning downstream of C4da neurons in responses to noxious stimuli.

In addition to mCSIs, both *R94B10-GAL4* and *R52F05-GAL4* drive weak expression in other neurons across the brain and the VNC (Figures 10A and 11). To confirm that the rolling behavior is triggered by the activation of mCSI and not the other neurons, I performed two additional experiments. First, I expressed TSH-GAL80, which suppresses GAL4 activity in VNC neurons (Berni et al., 2012; Clyne et al., 2008), in combination with R94B10-GAL4 and UAS-ReaChR. In this condition, red light application did not induce the rolling behavior (Figure 19A). This suggests that R94B10-GAL4 expressing neurons in the VNC, but not in the brain, are critical for the induction of the rolling behavior. Second, I expressed R94B10-GAL80 in combination with R52F05-GAL4 and UAS-ReaChR in the third instar larvae. This resulted in loss of ReaChR expression in mCSIs compared to larvae

harboring *R52F05-GAL4* and *UAS-ReaChR*. In these animals, no significant rolling behavior was observed upon red light application (Figure 19B), suggesting that neurons shared by the two *GAL4* lines are critical for triggering rolling behavior. These data further support the idea that mCSIs contribute to induction of the rolling behavior.

I next asked whether mCSIs function downstream of C4da neurons to induce the rolling behavior. In order to investigate that, I silenced mCSIs by using the tetanus neurotoxin light chain (TNT) which cleaves the synaptic vesicle-associated protein Synaptobrevin, thereby chronically blocking transmitter release (Sweeney et al., 1995). Red light application to larvae expressing ReaChR in C4da neurons triggered immediate and robust rolling behavior in a significant fraction of animals (Figure 20: Effector control, 62.3 %, n = 61). In contrast, silencing mCSIs in larvae expressing ReaChR in C4da neurons significantly decreased the probability of the rolling behavior in response to C4da activation (Figure 20: *R94B10 GAL4* control, 80.5%, n = 41; *R94B10* inhibition, 25.8 %, n = 31; *R52F05 GAL4* control, 62.1 %, n = 37; *R52F05* inhibition, 29.2 %, n = 24). This suggests that mCSIs constitute the nociceptive circuits to evoke the rolling behaviors upon C4da activation. From these data, I conclude that mCSIs are the second-order neurons of the nociceptive circuits that are necessary and sufficient to induce the rolling behavior.

mCSIs send output to motor neurons to evoke rolling behavior

A recent study identified a cluster of neurons in the VNC, designated as Basins, as the second-order interneurons of C4da neurons and suggested that Basins likely send output at least in part to Goro interneurons (Ohyama et al., 2015). Dual color labeling revealed that mCSIs are different from Basin and Goro neurons (Figure 21A). In addition, mCSl activation-induced rolling behavior was unaffected by Goro silencing (Figure 21B). Consistently, mCSl activation did not increase Ca^{2+} levels in Goro upon mCSIs activation (Figures 21D and 21E). Similarly, Basin activation-induced rolling behavior was unaffected by mCSI silencing (Figure 21C). Thus, mCSIs likely function in parallel with the Basin-Goro pathway.

Since mCSIs extend axons to the dorsal area in the neuropile which is innervated by motor neuron dendrites (Figures 10B and 16B), I reasoned that mCSIs might send output to motor neurons. To test this possibility, I performed dual labeling of *R94B10-LexA* and motor neuron-*GAL4* lines. I found a close apposition between mCSI axonal terminals and one of the motor-neuron expressing GAL4 lines, *BarH1-GAL4.* Bar-H1 GAL4 drives expression in SNa motor neurons in each abdominal segment (Sato et al., 1999; Garces et al., 2006) (Figures 22A and 22B). I thus performed Syb-GRASP between mCSIs and SNa neurons but failed to detect visible signal. However, my Ca^{2+} imaging revealed a robust Ca^{2+} elevation in SNa neurons upon mCSI activation (Figures 22C and 22D), implying that SNa neurons might be indirect functional downstream targets of C4da-mCSI pathway.

To further test whether SNa motor neurons function in the C4da-mCSI pathway, I examined the effects of silencing SNa motor neurons on larval response to C4da or mCSI activation. I optogenetically activated C4da neurons or mCSIs in larvae harboring *BarH1-*

GAL4 and *UAS-TNT*, and found that C4da/mCSIs induced rolling behavior was significantly reduced in larvae harboring *BarH1-GAL4* and *UAS-TNT* (Figures 23A and 23B). I likewise observed a significant reduction of C4da/mCSI nduced rolling behavior in larvae harboring *UAS-TNT* and *NP4099-GAL4*, which also drives expression in SNa motor neurons (Figures 23A, 23B, and 24). I observed no significant reduction in the crawling speed and the turn rate in larvae harboring *BarH1-GAL4* or *NP4099-GAL4* and *UAS-TNT* compared to control (Figures 23C and 23D). These data suggest that SNa motor neurons are essential for C4da activation-induced rolling behavior but not for basal locomotion. Taken together, my data suggest that the C4da-mCSI nociceptive circuits evoke rolling behavior, at least in part, through SNa motor neurons.

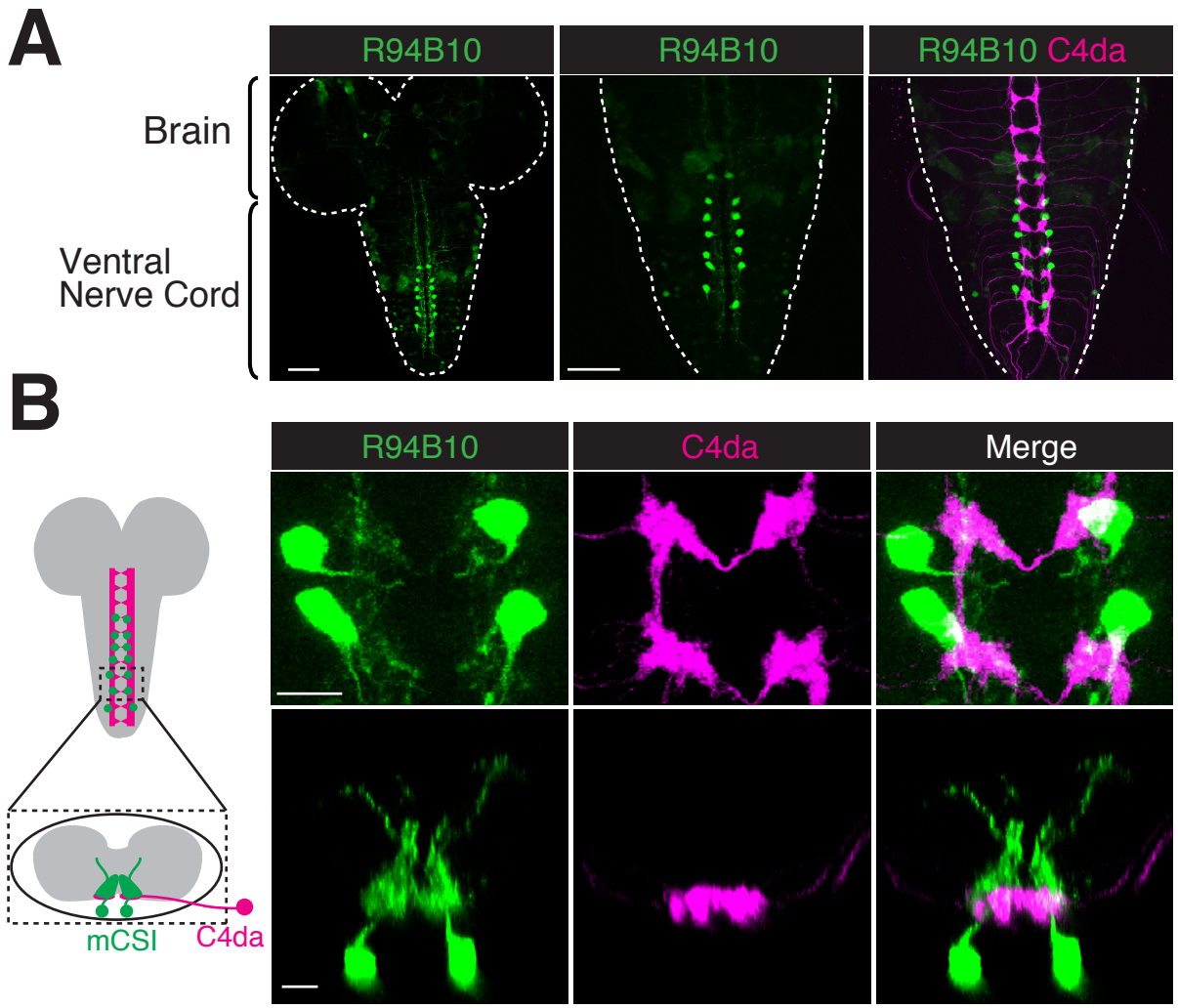

Figure 10. C4da axons and mCSI dendrites are closely apposed in the VNC

(A) Expression patterns of R94B10-GAL4 in the larval central nervous system. The right two panels show simultaneous labeling of the VNC with R94B10-GAL4, UAS-mCD8GFP (green) and the C4da marker ppk-CD4-tdTomato (magenta) in the third instar larvae. Genotype, *w; UAS-mCD8GFP/+; R94B10-GAL4/ppk-CD4-tdTomato*. Scale bars, 50 μm. (B) Simultaneous labeling of the larval VNC with R94B10-GAL4, UAS-mCD8GFP (green) and the C4da marker ppk-CD4-tdTomato (magenta). Top panels show magnified images of the abdominal A5-6 segments (the area indicated by the dotted lines in the schema) in the VNC. Note that R94B10-GAL4 drives mCD8GFP in a pair of neurons near the region occupied by C4da axon terminals, and their neurites overlapped with C4da axon terminals. Bottom panels show a transverse section of A5 segment. Note that ventral parts of R94B10-driving neurites (green) are overlapped with C4da axon terminals (magenta). Right panels show merged images. Genotype, *w; UAS-mCD8GFP/+; R94B10-GAL4/ppk-CD4-tdTomato*. Scale bars, 10 μm.

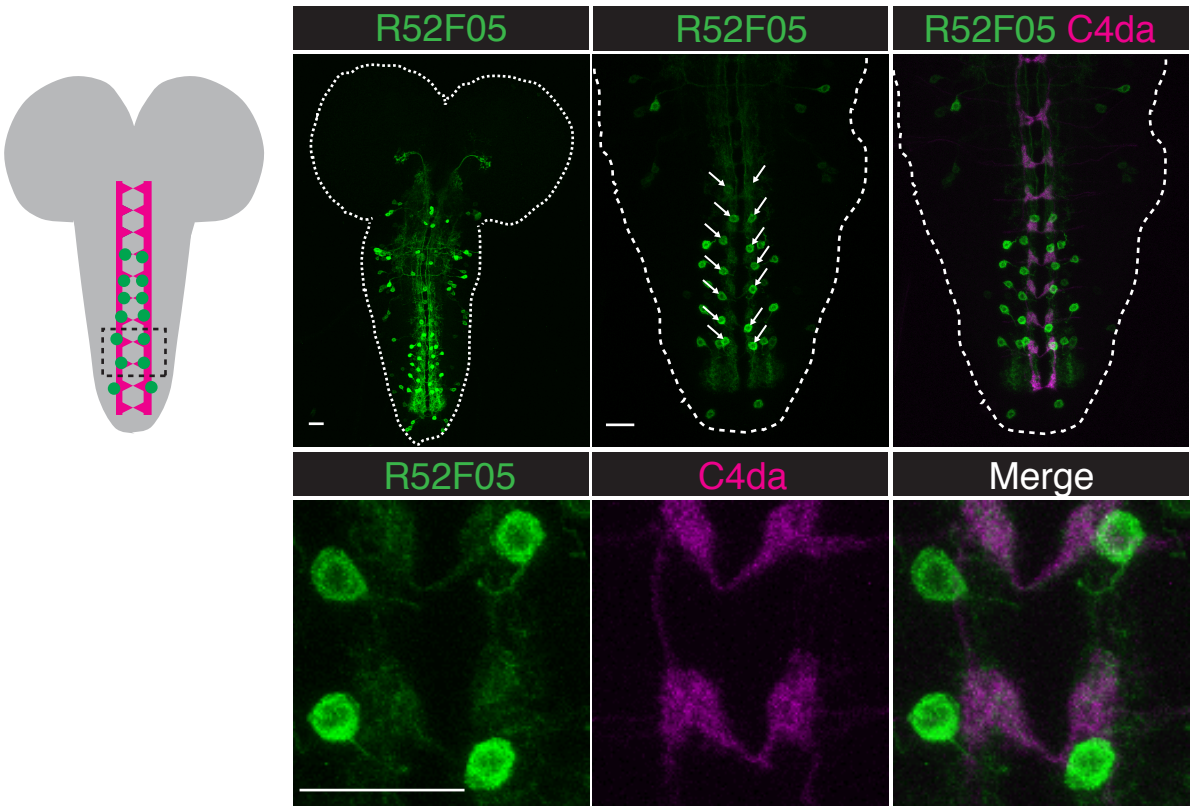

Figure 11. Expression patterns of R52F05-GAL4

R52F05-GAL4 drives mCD8GFP in a pair of neurons near the region occupied by C4da axon terminals and their neurites overlapped with C4da axon terminals (arrows). Bottom panels show magnified images of abdominal A5-6 segments (the area around the dotted lines in the schema) in the VNC. Genotype, *w; UAS-mCD8GFP/+; ppk-CD4-tdTomato/R52F05-GAL4*. Scale bars, 10 μm.

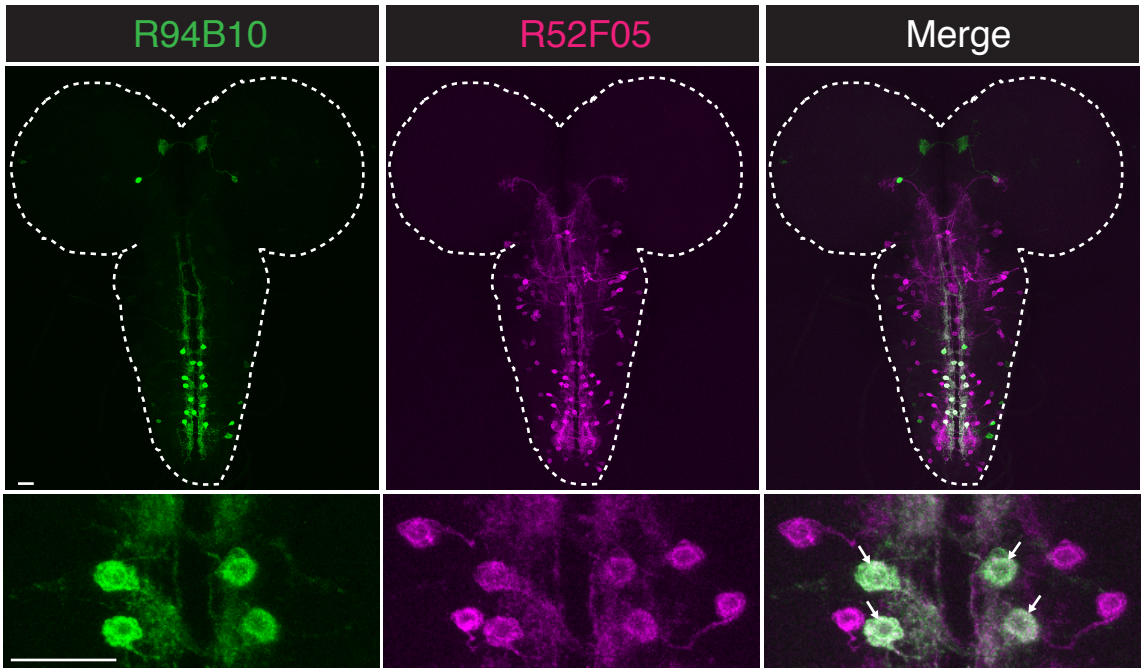

Figure 12. R94B10 and R52F05 labels same neurons, mCSI

Binary labeling revealed that R94B10-Lex, LexAop-mCD8GFP (green) and R52F05-GAL4, UAS-tdTomato (magenta) label the same neurons in the VNC. Bottom panels show magnified images of abdominal A3-4 segments in the VNC. Note that a pair of neurons in each abdominal segments are co-labeled by R94B10-Lex and R52F05-GAL4 (arrows). Genotype, *yw, LexAop-mCD8GFP,UAS-mCD8RFP/+; +/+; R94B10-LexA/R52F05-GAL4*. Scale bars, 10 μm.

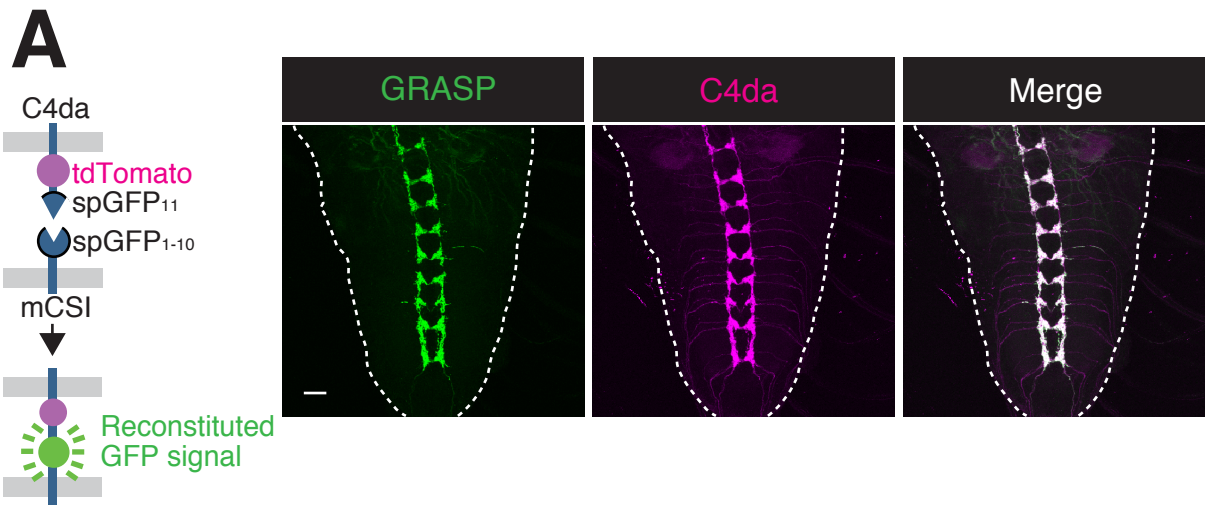
A
C4da
tdTomato
spGFP11
spGFP1-10
mCSI
Reconstituted
GFP signal
GRASP
C4da
Merge

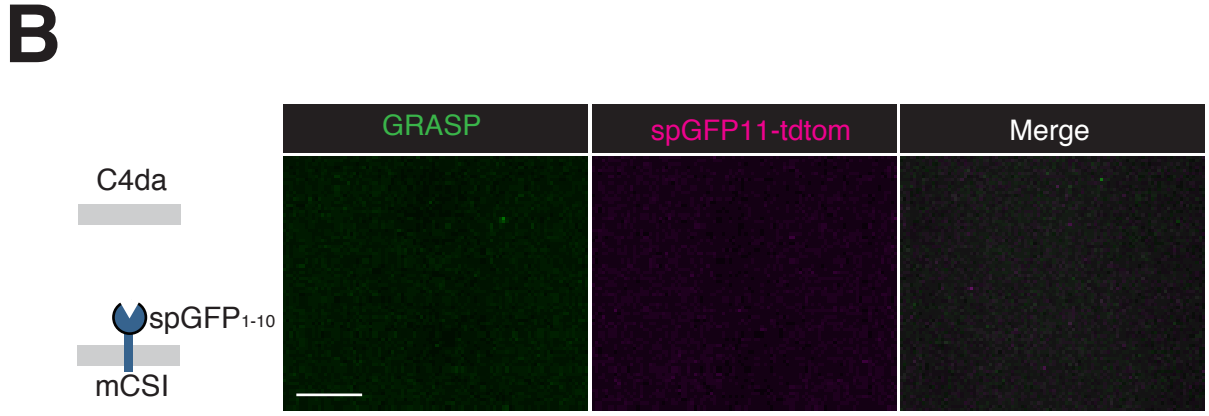
B
C4da
spGFP1-10
mCSI
GRASP
spGFP11-tdtom
Merge

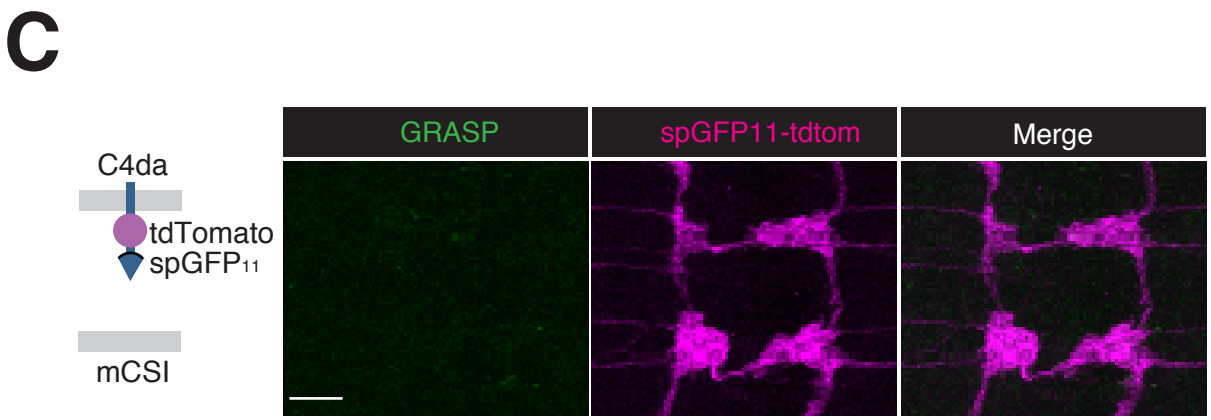
C
C4da
tdTomato
spGFP11
mCSI
GRASP
spGFP11-tdtom
Merge

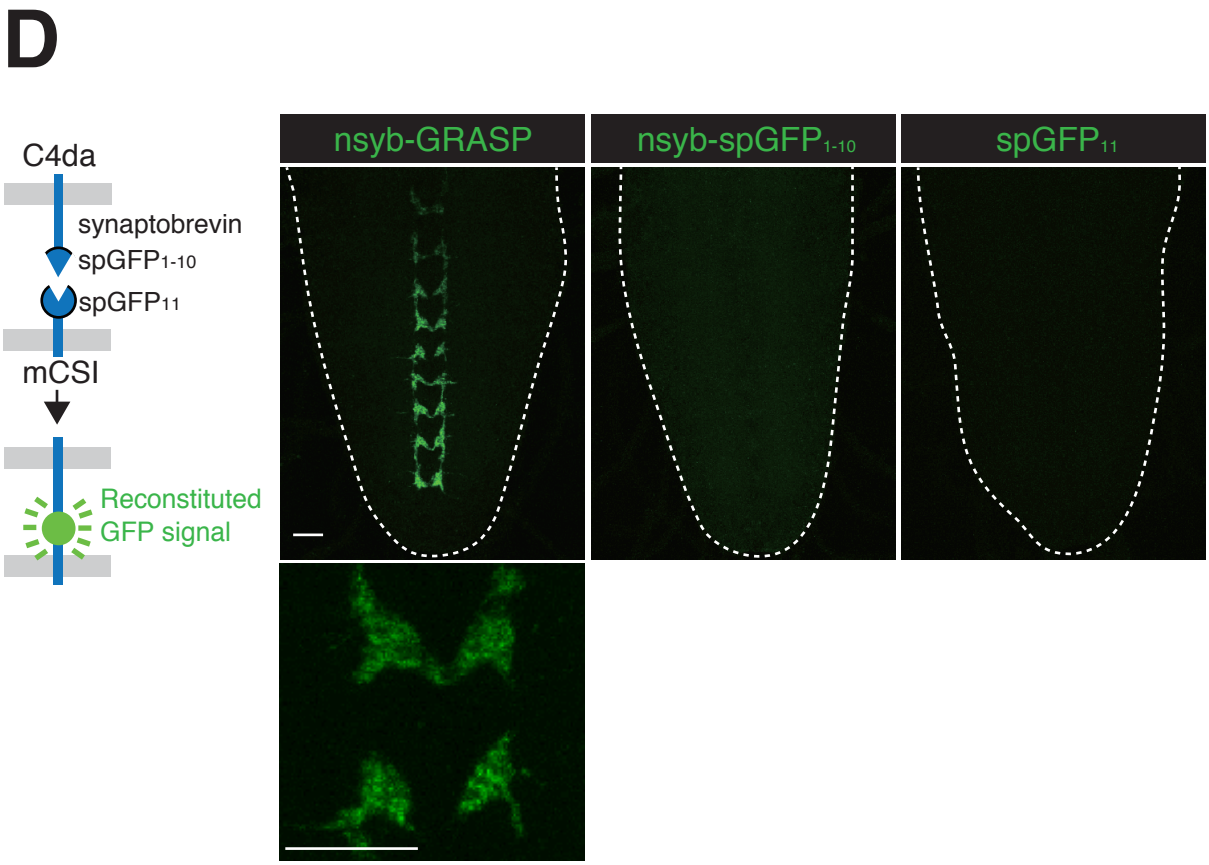

Figure 13. GRASP analysis between C4da neurons and mCSIs

(A) GRASP signals (green) obtained with C4da-LexA, LexAop-tdTomato-spGFP$_{11}$ (magenta) and R94B10-GAL4, UAS-spGFP$_{1-10}$ (no signal). Right panel shows the merged image. Genotype, *w; +/+; R94B10-GAL4/ppk-LexA, LexAop-spGFP$_{11}$-tdTomato, UAS-spGFP$_{1-10}$*. Scale bar, 20 µm.

(B and C) No significant GRASP signal was detected in the VNC when either of the split GFP fragment alone was expressed in mCSIs (A) or C4da neurons (B). Genotypes, *w; +/+; R94B10-GAL4/LexAop-spGFP$_{11}$-tdTomato, UAS-spGFP$_{1-10}$* (A) and *w; +/+; ppk-LexA, LexAop-spGFP$_{11}$-tdTomato, UAS-spGFP$_{1-10}$/+* (B). Scale bars, 10 µm.

(D) Syb-GRASP between C4da neurons and mCSIs shows specific GFP reconstruction along C4da axonal tracks in the VNC. Genotypes, *w; UAS-nsyb-spGFP$_{1-10}$, LexAop-CD4-spGFP$_{11}$/ ppk-GAL4; R94B10-LexA/+* (left), *w; UAS-nsyb-spGFP$_{1-10}$, LexAop-CD4-spGFP$_{11}$/ppk-GAL4; +/+* (middle) and *w; UAS-nsyb-spGFP$_{1-10}$, LexAop-CD4-spGFP$_{11}$/+; R94B10-LexA/+* (right). Scale bar, 20 µm.

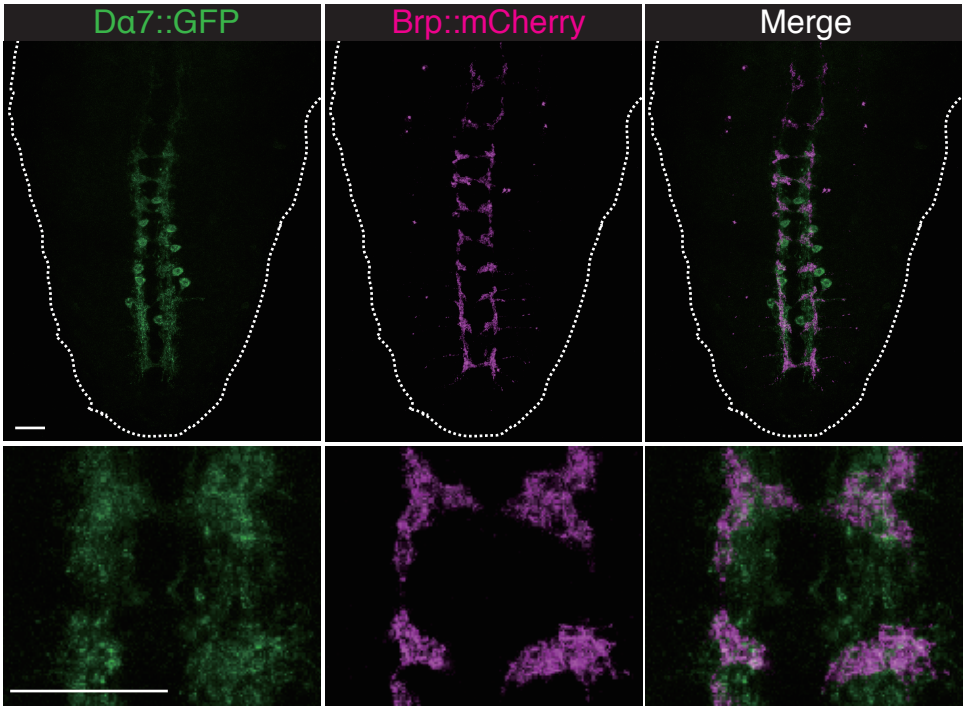

Figure 14. Postsynaptic marker in mCSIs is colocalized with C4da presynaptic marker

Binary labeling revealed that R94B10-GAL4, UAS-Dα7-GFP (green) and R27H06-LexA, LexAop-Brp-short-mCherry (magenta) are compartmentalized into similar locations in the VNC. Bottom panels show magnified images of abdominal A4-5 segments in the VNC. Scale bars 20 μm.

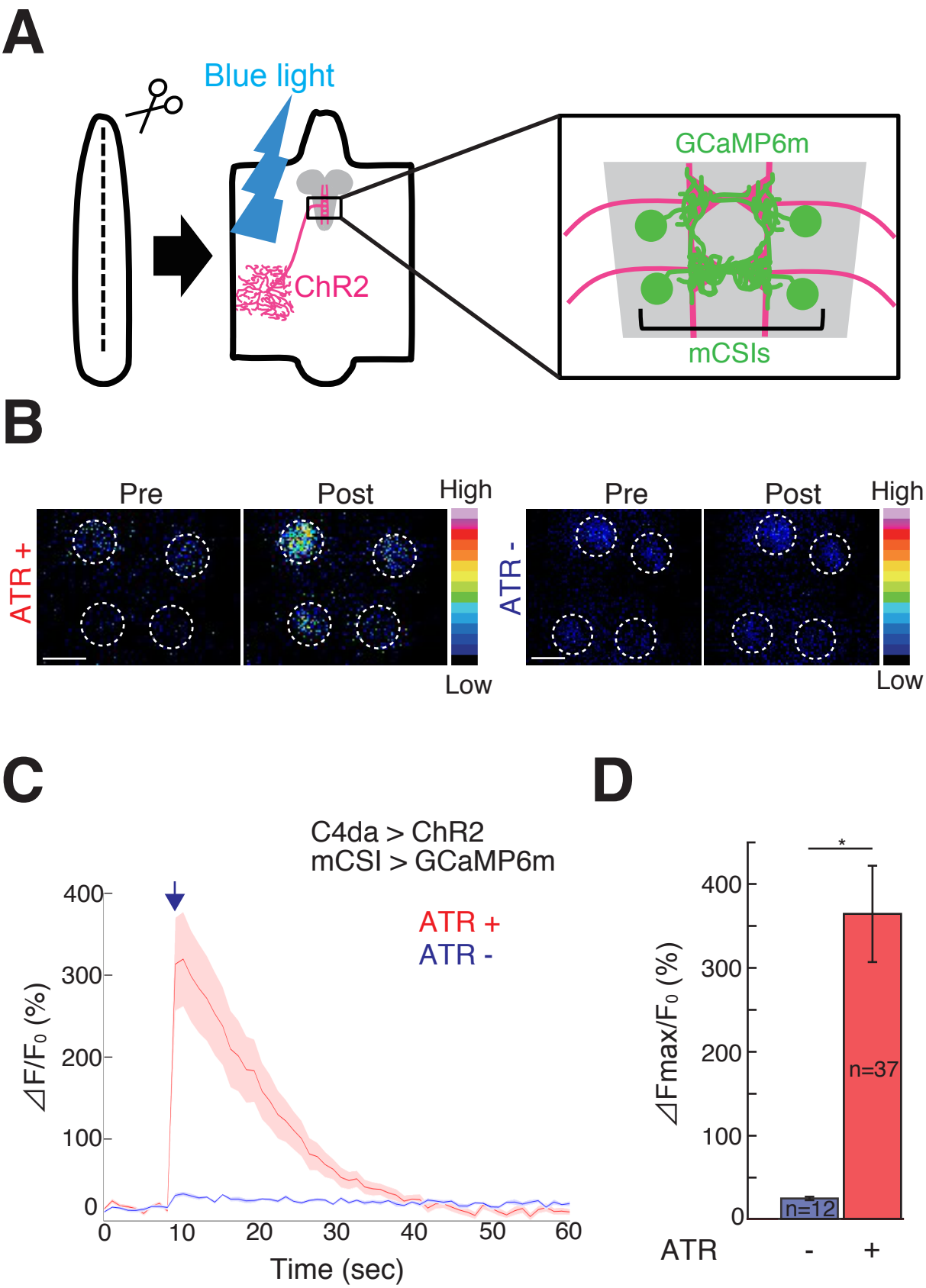
A
Blue light
ChR2
GCaMP6m
mCSIs
B
Pre
Post
High
Low
ATR +
ATR -
C
C4da > ChR2
mCSI > GCaMP6m
ATR +
ATR -
ΔF/F0 (%)
Time (sec)
D
ΔFmax/F0 (%)
n=37
n=12
ATR
-
+
*

Figure 15. Optogenetic stimulation of C4da neurons elicits calcium response in mCSIs
(A) Schematic images of preparations for calcium imaging of mCSIs upon C4da activation in a larval fillet.
(B) Ca^{2+} imaging of mCSIs upon C4da activation in ATR + (left panels) and ATR - (right panels) conditions. Representative images of relative Ca^{2+} levels 2 sec before (pre) and 2 sec after (post) light application are shown. Scale bars, 10 μm.
(C) Time series of the calcium response in mCSIs upon optogenetic activation of C4da neurons. Blue light application started at the time indicated by arrow and continued for 2 sec. During the activation, images were not acquired to avoid the halation of the images. n = 37 for ATR + and n=12 for ATR -, envelopes indicate ±SEM.
(D) Average of mCSI $\Delta F_{max}/F_0$ values. Data are shown as the mean ± SEM. Statistical significance was assessed by Welch's t-test, *$p < 0.05$.

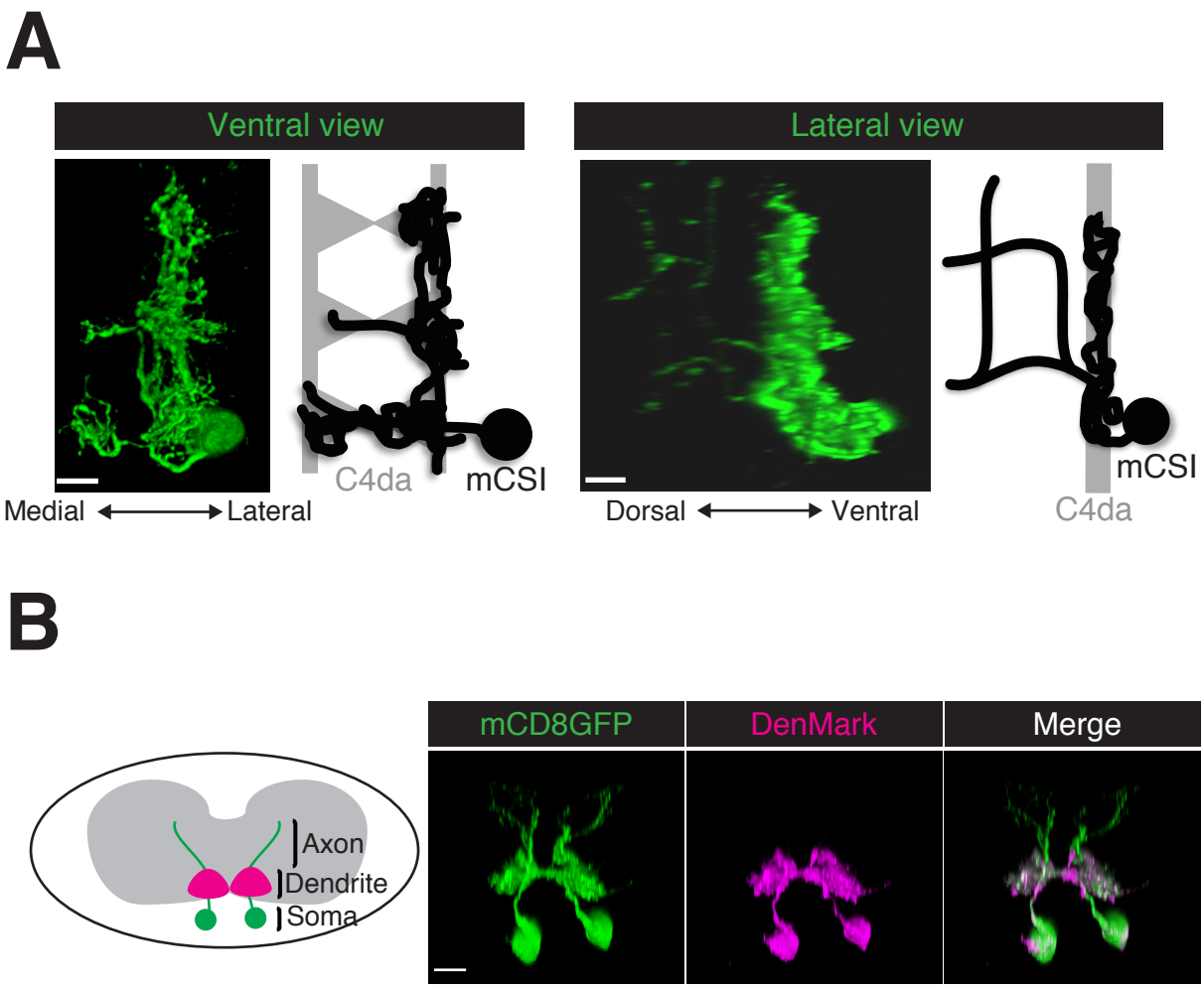

Figure 16. mCSIs extend axons toward the dorsal neutrophil region

(A) Flip-out analysis of single mCSIs. Scale bars, 10 μm.

(B) Simultaneous expression of mCD8GFP and the dendrite marker DenMark (magenta) in mCSIs. Note that neurites extending toward the dorsal neuropile region are DenMark negative whereas ventral branches are DenMark positive, indicating that dorsal and ventral neurites are axons and dendrites, respectively.

Genotype, *w; UAS-DenMark/+; R94B10-GAL4, UAS-mCD8GFP/+*. Scale bar, 10 μm.

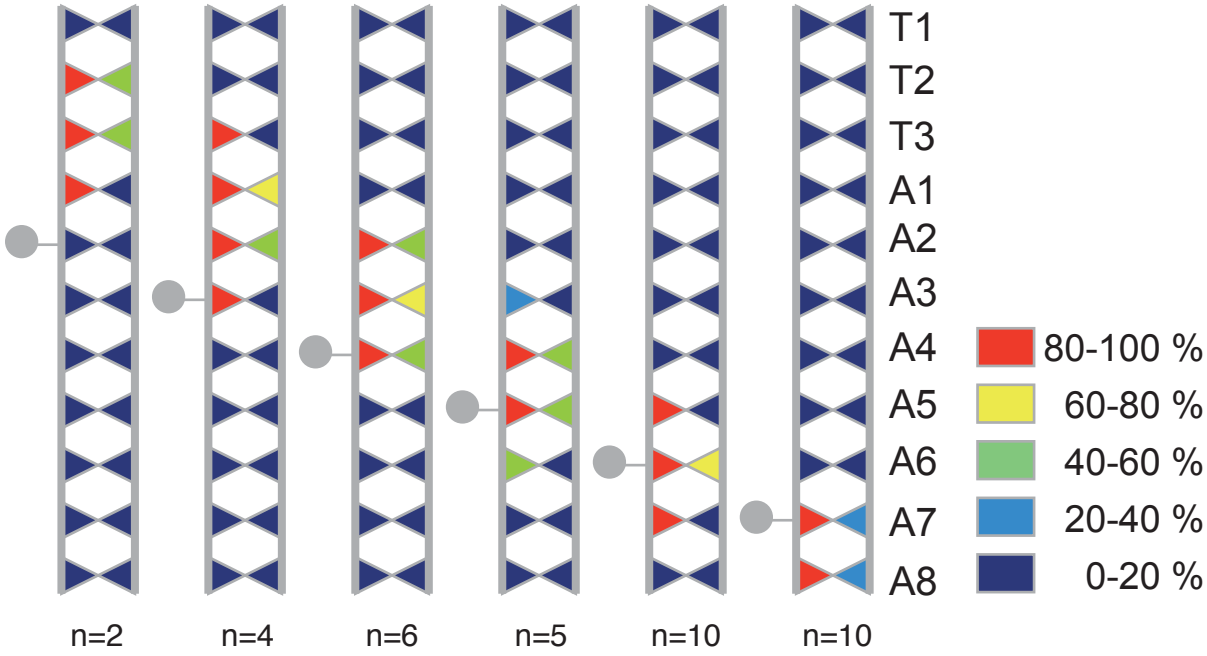

Figure 17. The segmental organization of mCSIs in the VNC

Each diagram shows mCSI dendrite innervation pattern.Note each mCSI innervates a limited number of segments. The pseudo-color represents the ratio of mCSI dendrites innervating particular abdominal segments. The data was obtained by Dr. Rei Morikawa.

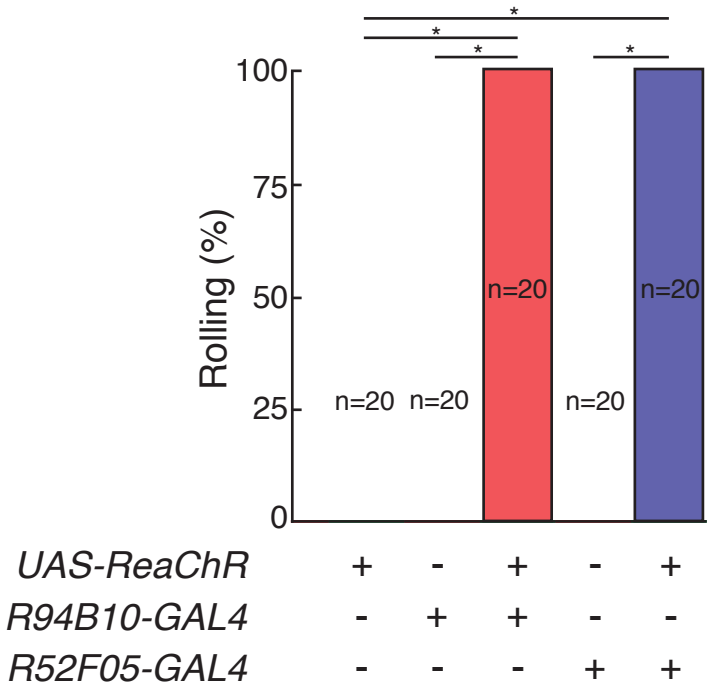

Figure 18. R94B10 and R52F05 labeled neurons are sufficient for rolling behavior
Optical activation of mCSIs triggers rolling behavior in the third instar larvae. Statistical significance was evaluated by Fisher' s exact test with Benjamini-Hochberg correction. *$p < 0.05$.

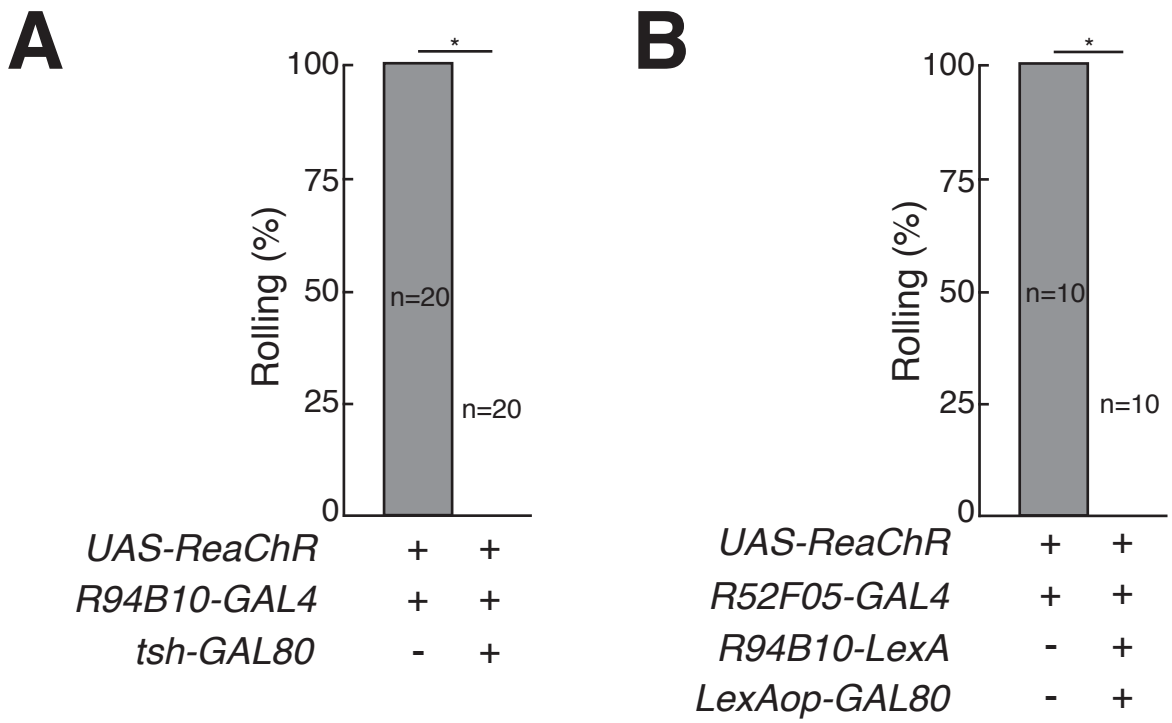

Figure 19. mCSIs are responsible for rolling behavior

(A) mCSI activation-induced rolling behavior was completely abolished by tsh-GAL80. Statistical significance was evaluated by Fisher' s exact test. *$p < 0.05$.

(B) mCSI activation-induced rolling behavior was completely abolished by R94B10-GAL80. Statistical significance was evaluated by Fisher' s exact test. *$p < 0.05$.

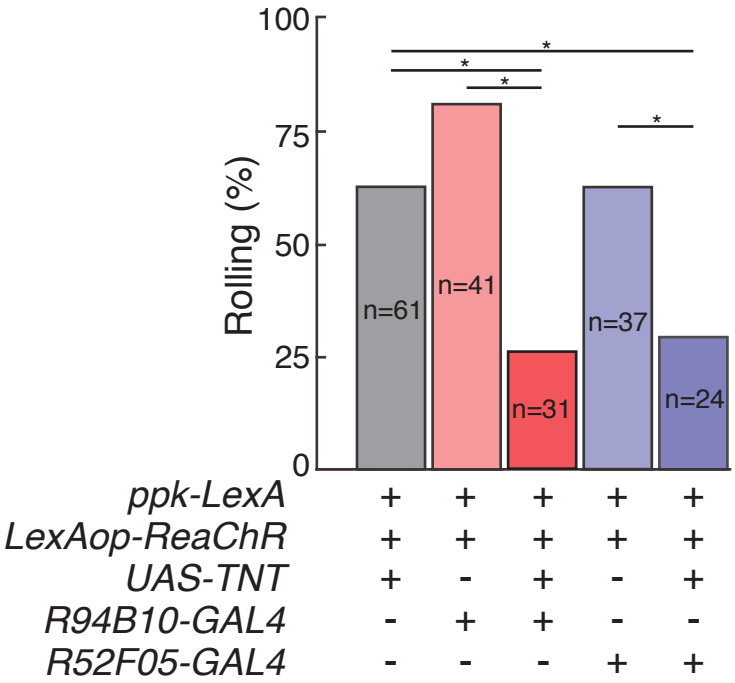

Figure 20. mCSIs are necessary for rolling behavior

Silencing mCSIs causes a significant reduction of rolling probability upon C4da activation. Statistical significance was evaluated by Fisher' s exact test with Benjamini-Hochberg correction. *$p < 0.05$.

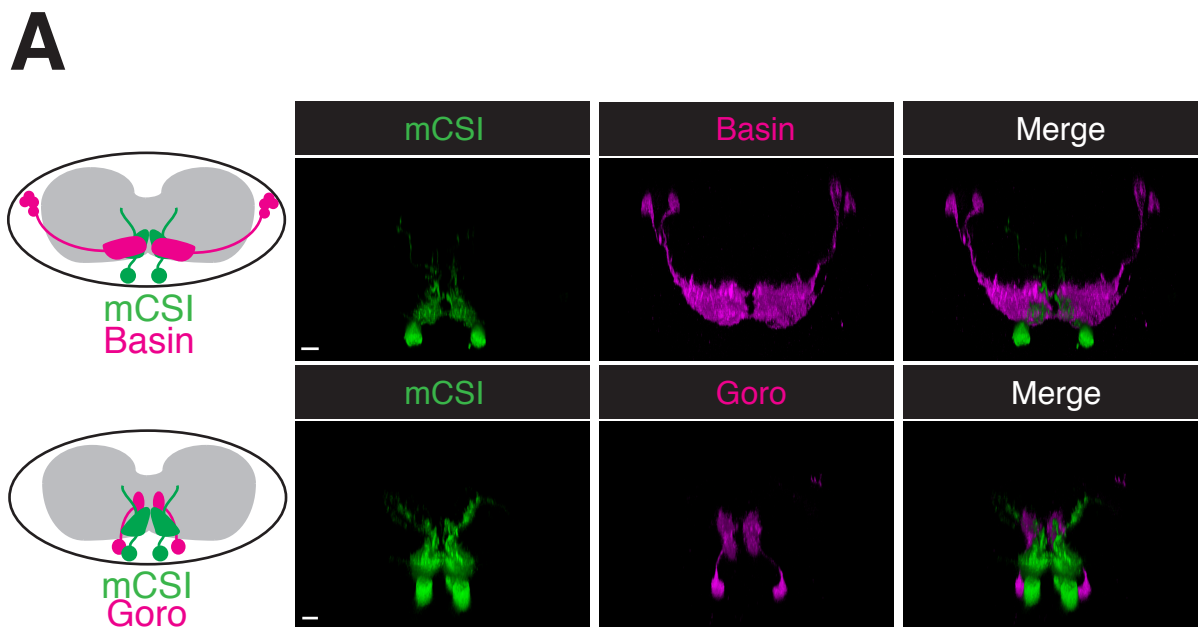
A
mCSI
Basin
Merge
mCSI
Goro
Merge
mCSI
Basin
mCSI
Goro

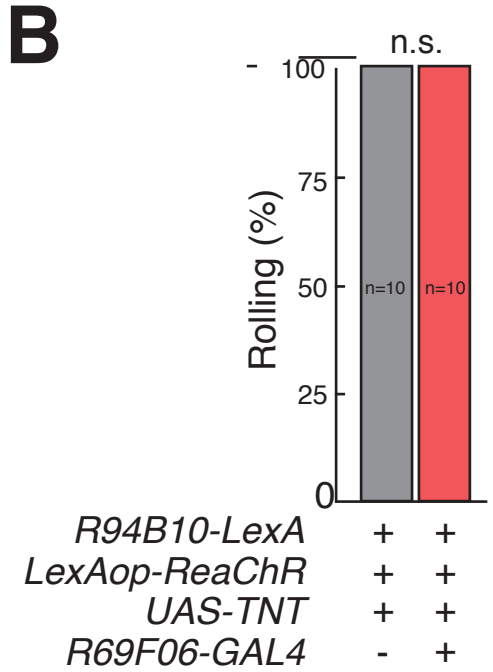
B
n.s.
Rolling (%)
100
75
50
25
0
n=10
n=10
R94B10-LexA + +
LexAop-ReaChR + +
UAS-TNT + +
R69F06-GAL4 - +

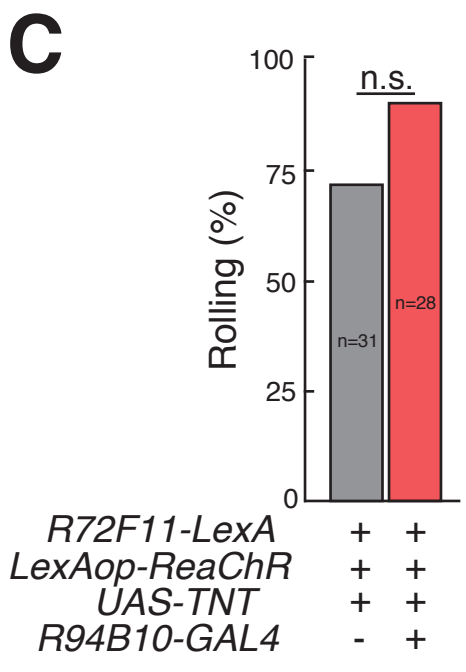
C
n.s.
Rolling (%)
100
75
50
25
0
n=31
n=28
R72F11-LexA + +
LexAop-ReaChR + +
UAS-TNT + +
R94B10-GAL4 - +

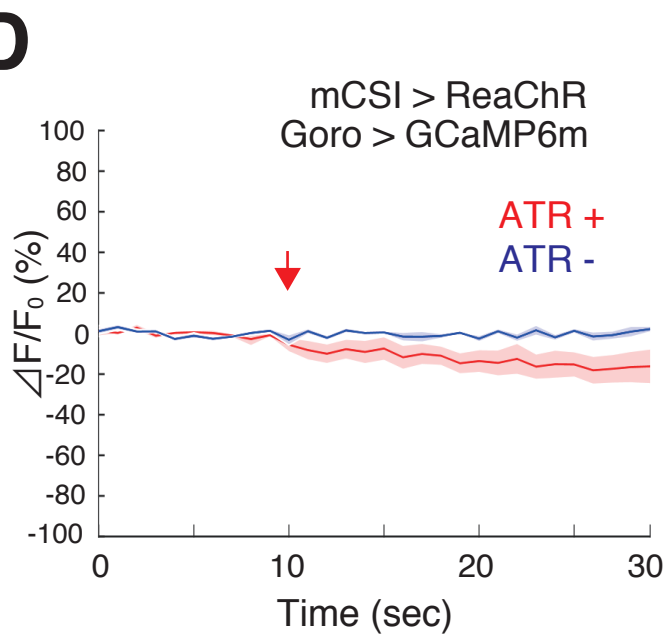
D
mCSI > ReaChR
Goro > GCaMP6m
ATR +
ATR -
ΔF/F0 (%)
100
80
60
40
20
0
-20
-40
-60
-80
-100
0
10
20
30
Time (sec)

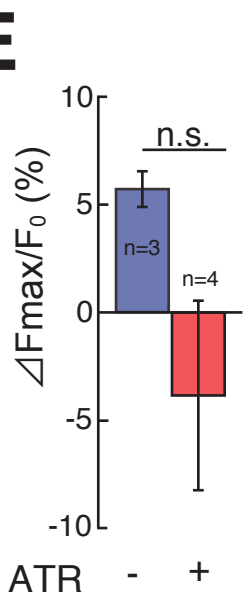
E
n.s.
ΔFmax/F0 (%)
10
5
0
-5
-10
n=3
n=4
ATR - +

Figure 21. mCSI acts in parallel with Basin-Goro pathway

(A) Projection patterns of mCSIs (green) and Basins (magenta) or Goro nerons (magenta) in A5 segments for Basins and A1-2 segments for Goro. Genotypes, *w; R72F11-LexA/LexAop-CD2RFP; R94B10-GAL4/UAS-mCD8GFP* (for mCSIs and Basins) and *yw, LexAop-mCD8GFP, UAS-mCD8RFP/+*; +/+; *R94B10-LexA/R69F06-GAL4* (for mCSIs and Goros). Scale bars, 10μm.

(B) mCSI activation-induced rolling behavior was unaffected by Goro silencing. Statistical significance was assessed by Fisher's exact test. *p<0.05.

(C) Basin activation-induced rolling behavior was not significantly affected by mCSI silencing. Statistical significance was assessed by Fisher's exact test. *p<0.05.

(D) Time series of calcium response of Goro neurons upon optogenetic activation of mCSIs. Red light application started at the time indicated by the arrow and continued for 2 sec. During the activation, images were not acquired to avoid the halation of the images. ATR (-), n=3; ATR (+), n=4; Envelopes indicate ± SEM.

(E) Average of Goro $\Delta Fmax/F_0$ vaues. Data are shown as the mean ± SEM. Statistical significance was assessed by Welch's t-test. *p<0.05.

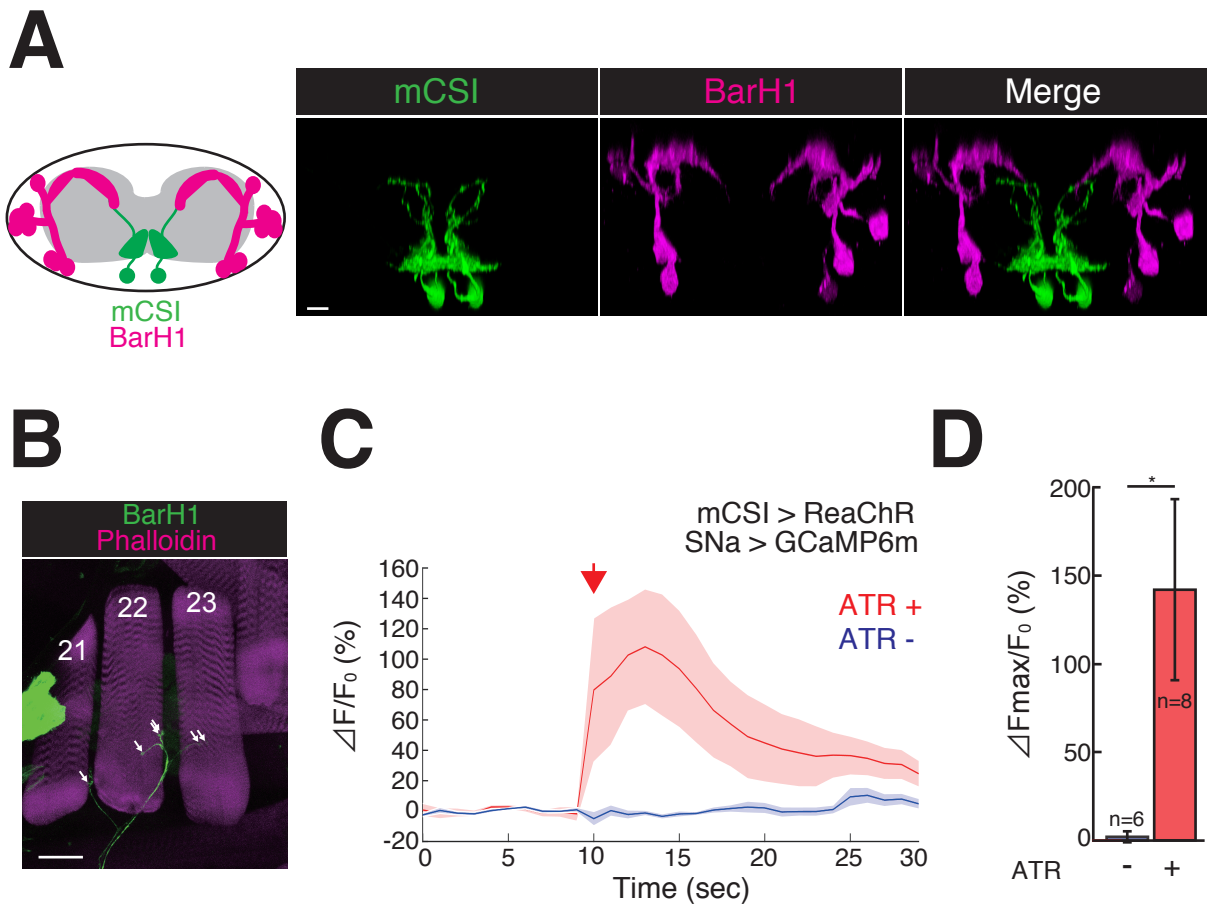

Figure 22. mCSIs send output to SNa motor neurons

(A) Dual labeling of mCSIs (R94B10-LexA, LexAop-mCD8GFP: green) and SNa motor neurons (BarH1-GAL4, UAS-mCD8RFP: magenta). A transverse section of A5 segment is shown. Note that mCSI axonal terminals and SNa dendritic branches are closely apposed. Genotype, *BarH1-GAL4/ LexAop-mCD8GFP, UAS-mCD8RFP; +/+; R94B10-LexA/+*. Scale bar, 10 µm.

(B) Axonal projection of BarH1-GAL4 labeled motor neurons onto muscles in the third instar larva. Arrows indicate presynaptic sites. Scale bar, 50 µm. This data was obtained by Dr. Eri Hasegawa.

(C) Time series of calcium responses of SNa motor neurons upon optogenetic activation of mCSIs. Red light application was started at the time indicated by the arrow and continued for 2 sec. During the activation, images were not acquired to avoid the halation of the images. ATR (-), n = 6; ATR (+), n = 8; Envelopes indicate ± SEM.

(D) Average of mCSI $\Delta F_{max}/F_0$ values. Data are shown as the mean ± SEM. Statistical significance was assessed by Welch's t-test, *$p < 0.05$.

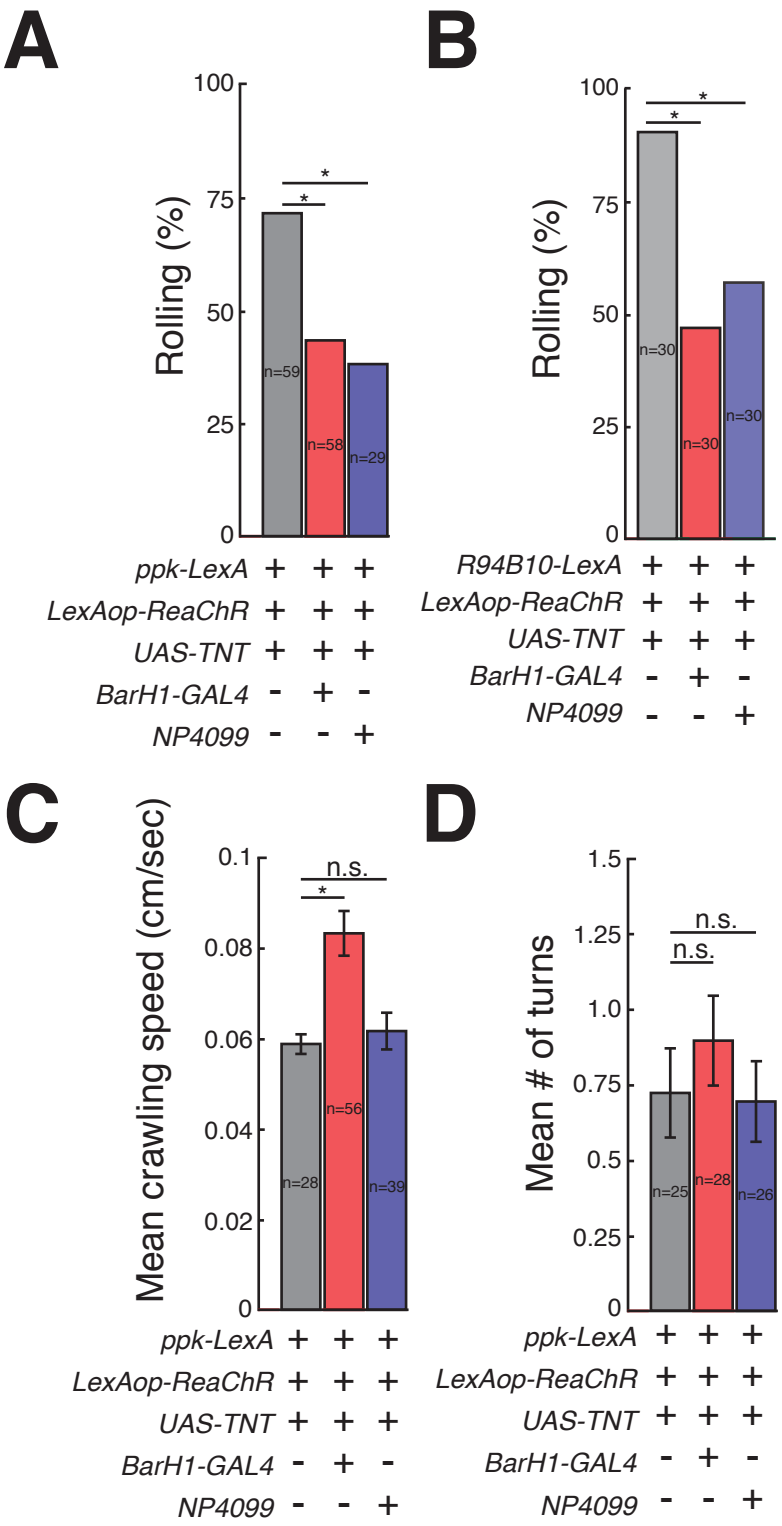

Figure 23. SNa motor neurons function in the C4da-Rolling pathway

(A and B) Probability of rolling behavior upon C4da (A) or mCSI (B) activation in control (gray), and in SNa-silenced larvae (red and blue). Statistical significance was evaluated by Fisher' s exact test with Benjamini-Hochberg correction. *p< 0.05.

(C and D) Basal Crawling speed (C) and turn numbers (D) in control (gray) and SNa-silenced larvae (red and blue). Data are shown as the mean ± SEM. Statistical significance was evaluated by Welch' s t-test with Benjamini-Hochberg correction. *p < 0.05.

Figure 24. NP4099 labels SNa motor neurons

Expression patterns of mCSIs-Lex (green) and NP4099-GAL4 (magenta) in A5 segment.

Note that NP4099-GAL4 drives expression in SNa motor neurons in the VNC.

Genotype, *yw, LexAop-mCD8GFP, UAS-mCD8RFP/NP4099-GAL4; +/+; R94B10-LexA/+*.

Scale bar, 10 μm.

Discussion

In this study, by combining anatomical, physiological and behavioral analysis, I have identified local circuits that tranform noxious stimuli into the escape behavior in *Drosophila* larvae. Anatomical analysis indicates mCSIs inVNC are innervated by C4da neurons (Figures 10 and 13). Furthermore, mCSIs are activated upon optogenetic activation of C4da neurons, suggesting mCSIs are second-order neurons of C4da neurons (Figure 15). In addition, behavioral analysis reveals that mCSIs are necessary and sufficient for rolling behavior evoked by C4da neurons (Figures 18, 19 and 20). My data also suggest that mCSIs send output at least in part to SNa motor neurons to evoke the rolling behavior (Figures 22 and 23).

Segmental organization of mCSI

C4da neurons show a somatotopic map, the correspondence between position of soma and projection area in the VNC. The C4da neuron in the A1 segment on the body wall innervates mainly the A1 segment in the VNC (Grueber et al., 2007; Morikawa et al., 2011). Given that mCSIs elaborate their dendrites mainly in the segment where their soma exist (Figures 16 and 17), the somatotopic information is retained in this layer. However, single mCSI extends its dendrites to neighboring segments and are innervated by multiple C4da neurons in the different segments (Figure 17). This segmental organization implies that mCSIs might receive nociceptive information from multiple C4da neurons and integrate the signals to evoke robust escape behavior.

SNa motor neuron as functional downstream of mCSI

Calcium imaging and behavioral analysis indicate that SNa motor neurons are

functional downstream of mCSI (Figures 22 and 23). This finding is consistent with the previous report that SNa neurons in the abdominal segments are essential for self-righting, a behavior to correct its orientation if turned upside-down, rolling-like behavior but not for basal locomotion and turning behavior in *Drosophila* larvae (Picao-Osorio et al., 2015). SNa motor neurons innervate transverse muscles (Figures 22B and 25), suggesting muscle contraction of this direction generates the force to roll. However, I did not show that SNa motor neurons are more important than other motor neurons. Rolling is complex behavior and probably many muscles are involved in this behavior. What kind of muscles are used in this behavior are interesting remaining question.

Parallel pathways for nociceptive rolling behavior

Several experiments indicate mCSIs function in parallel to the Basin-Goro pathway to control the rolling behavior control. First, axons of mCSI seems not targeted to Goro (Figure 21A). Second, inhibition of Goro does not affect the probability of the mCSI- evoked rolling behavior (Figure 21B). Similarly, probability of the Basin-evoked rolling behavior was not affected by inhibition of mCSI (Figure 21C). Finally, the calcium level of Goro was not elevated upon activation of mCSI (Figures 21D and 21E). Given that Basin-Goro pathway acts to integrate nociceptive signal detected by C4da neurons and vibration signal detected by ch neurons (Ohayama et al., 2015), and that the silencing of mCSI significantly reduces the probability of the rolling behavior evoked by activation of C4da neurons alone, mCSI seems to be a pathway important for detecting nociceptive signals that activate C4da neurons alone. Further structural and functional studies of the nociceptive circuits should help to elucidate how multiple circuits collaborate to generate the stereotyped rolling behavior.

mCSI as uni- or multi-sensory second order neuron

Another type of second-order neuron, Basin (Figures 6 and 21A), receives input from ch neurons and C4da neuron. It is conceivable that mCSI also receives input from multiple sensory neurons. Based on the central projection pattern of sensory neurons (Kohsaka et al., 2012)(Figure 26), I speculate the existence of the sensory neurons that can input to mCSI.

mCSIs dendrites occupy the C4da axon terminal region (Figure 10B). These dendrites modestly extend laterally where axons of classⅢ da neurons terminate. Thus, there is a possibility that mCSI also receives inputs from classⅢ da neurons. However, considering that the mCSIs inhibition results in a significant reduction of rolling behavior triggered by stimulation of nociceptive C4da neurons alone (Figure 20) and that their laterally extending dendrites are not so dense amount compared with those innervating the C4da terminal region, they might mainly receive input from C4da neurons. Future studies, especially electron microscopy analysis, would reveal whether other sensory neurons input to mCSI or not.

mCSI send output to SNa directly or indirectly

In the dual labeling experiment, I found a close apposition between mCSI axon terminal and dendrites of SNa motor neurons (Figure 22A). To examine whether mCSIs directly send output to SNa motor neurons, I performed syb-GRASP but failed to detect obviously visible signal. However, it does not mean mCSI-SNa interaction is indirect. In syb-GRASP method, splitGFP$_{1-10}$ is fused with a component of synaptic vehicle synaptobrevin. In this method, GRASP signals are detected only when synaptic vehicles are fused to neuronal membrane upon calcium entry to presynaptic site, thus indicating excitation of the neuron

(Macpherson et al., 2015). The larvae raised on standard medium at 25℃ never exhibited rolling behavior suggesting a rolling mediating neural circuit, mCSI-SNa, is silent at any time. There is possibility that I could not obtain syb-GRASP signals for this reason. Future studies, for example electron microscopy analysis, would help to conclude whether mCSI-SNa interaction is direct or not.

Comparison of neural circuit for nociception between *drosophila* and vertebrate

In this study, I identified C4da-mCSI-SNa neural circuit for nociceptive rolling behavior. Although whether the mCSI-SNa interacts directly or not remains unclear, mCSI seems to send their output locally toward motor domains in the dorsal region of the VNC (Figures 10B and 16B). The simple circuit structure of the C4da-mCSI-motor neuron pathway is analogous to the local circuit in the mammalian spinal cord, which mediates the quick and robust escape behavior such as flexion reflex (Iggo et al., 1985; Cordero-Erausquin et al., 2016)(Figure 1). By contrast, in the Basin-Goro pathway, Basin interneurons receive convergent inputs, which are subsequently transduced to two or more additional interneurons upstream of Goro interneurons (Ohyama et al., 2015, Figure 6). Under the assumption that C4da-mCSI-SNa pathway is analogous to the mammalian reflex circuit, existence of several additional interneurons can be predicted. The mammalian nociceptive sensory signal activates divergent polysynaptic reflex pathways. One pathway excites motor neurons innervating flexor muscles of the stimulated limb, whereas another inhibits motor neurons that innervate the limb's extensor muscles (reciprocal innervation, Figure 27). Thus, there could be interneurons that inhibit activity of muscles other than SNa motor neurons in *Drosophila* nociceptive circuit. Second, mammalian reflex can produce the opposite effect in the contralateral limb, excitation of extensor motor neurons and inhibition of flexor motor

neurons (crossed-extension, Figure 27). This mechanism serves to enhance postural support during withdrawal of the stimulated limb. Therefore there could be interneurons in *Drosophila* nociceptive circuit which inhibits the activity of SNa motor neurons on the contralateral side.

Physiological stimulation which can activate mCSI

In this study, I employed optogenetics to activate C4da sensory neurons. Considering C4da neurons are polymodal nociceptors activated by intense thermal, mechanical or noxious light, it is important to identify which or all of them can activate mCSI. In other words, whether the dedicated circuits for thermo, mechanical and light nociception exists or not. Recent study suggests that the firing pattern of C4da neurons and resulting behaviors are different between thermo and light stimulation (Terada et al., 2016). In thermal nociception, C4da neurons exhibit burst and pause pattern of firing and the resulting output behavior is rolling. In light nociception, C4da neuron's firing rate is smaller than that in thermo-stimulation and the result is avoidance from the light.

Considering mCSIs were not activated by blue light stimulation to C4da neurons (Figure 15, ATR-), mCSIs are not involved in light mediated escape behavior. Thus, there is a possibility that only the burst and pause firing can excite mCSI which is necessary and sufficient for rolling behavior (Figure 28).

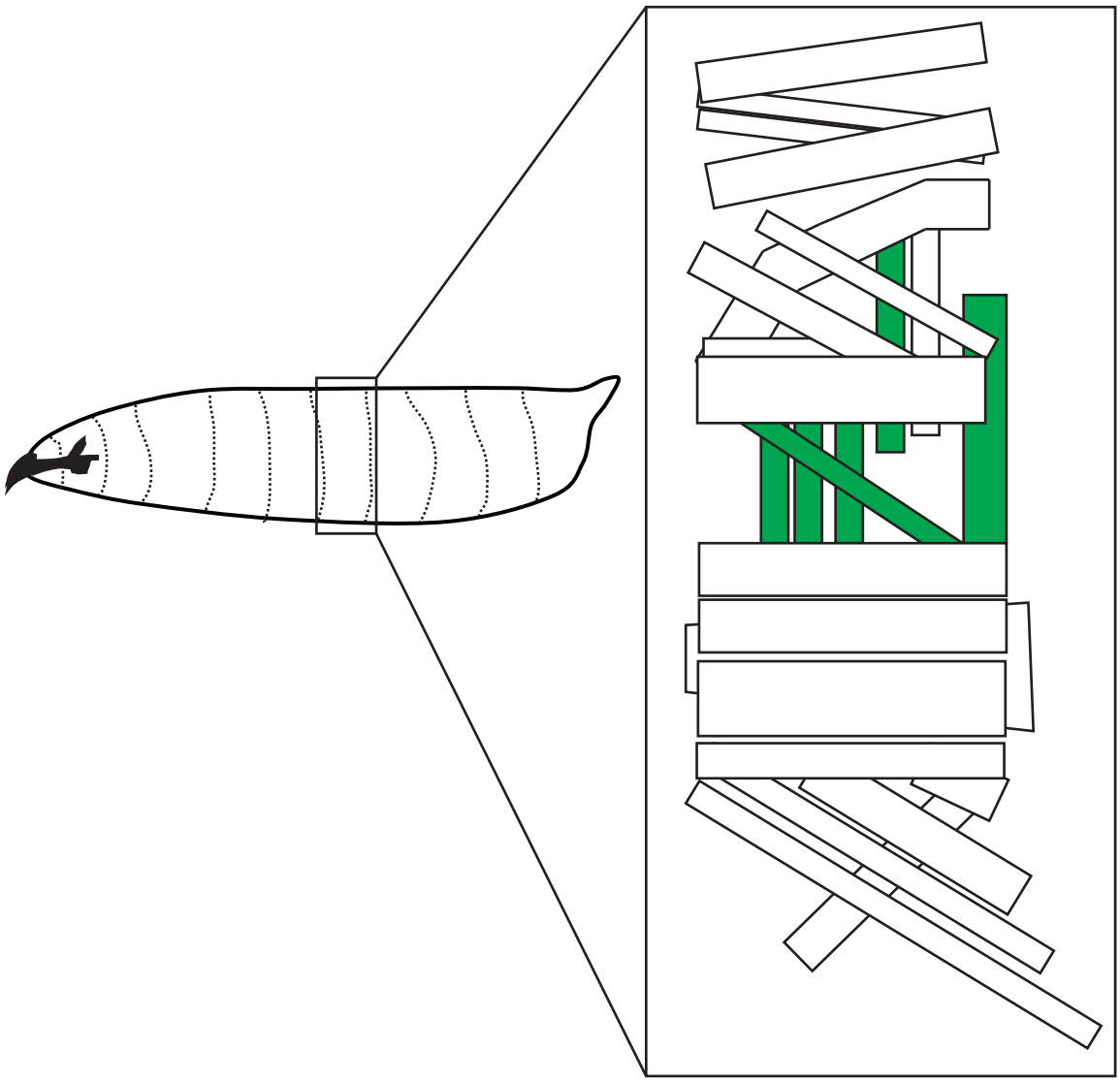

Figure 25. Muscles of the *Drosophila* larvae

Each rectangle represents a mucle of the abdominal segment. The rectangles colored green represent muscles innervated by SNa motor neurons.

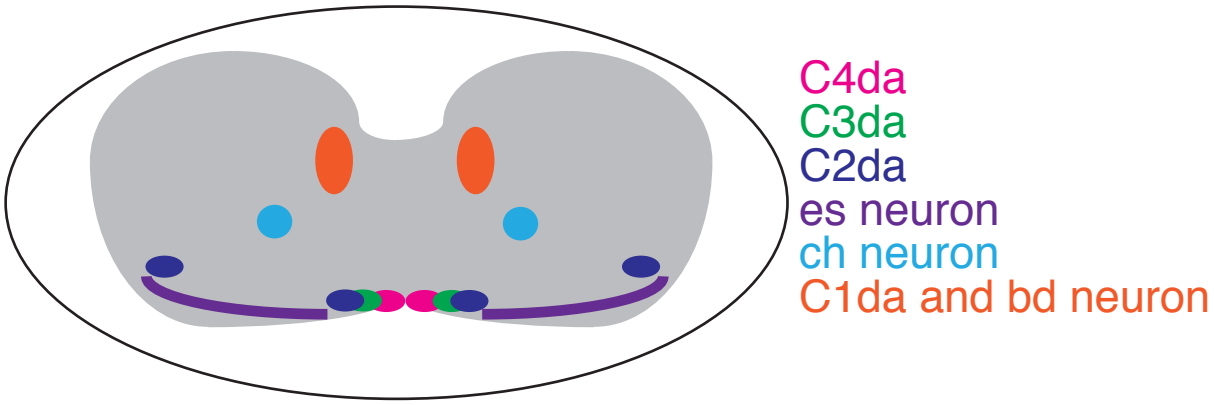

Figure 26. Central projection pattern of sensory neurons

Schematic representation of the VNC. Each color indicates the identity of sensory neurons. C4da neuron (magenta), C4da neuron (green), C2da neuron (deep blue), es neuron (purple), ch neuron (light blue), C1da and bd neuron (orange).

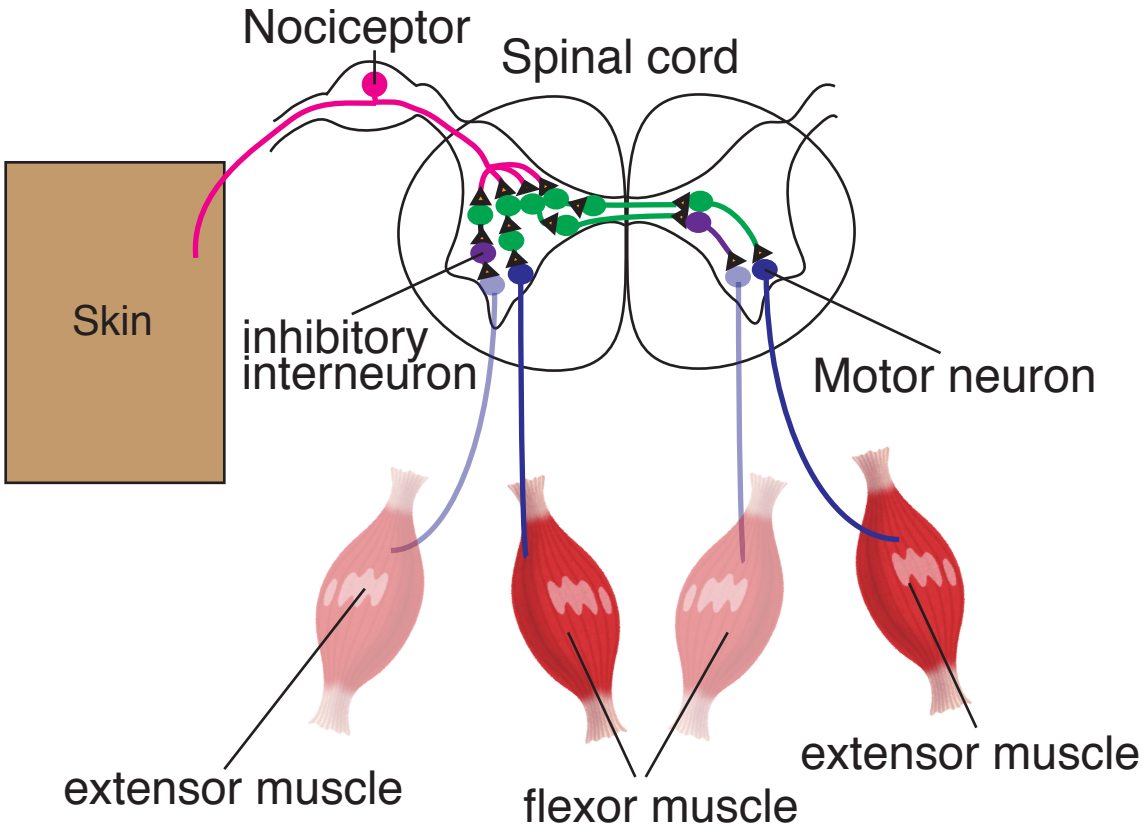

Figure 27. Vertebrate reflex circuit

Polysynaptic pathways in the spinal cord mediate the reflex. One excitatory pathway activates motor neurons which innervate flexor muscles on ipsilateral side, which then leads to withdrawal the limb from noxious stimuli. Another pathway simultaneously activates motor neurons innervating contralateral extensor muscles, provinding support during withdrawal of the limb. Inhibitory interneurons act to inactivate antagonistic muscles during the reflex response.

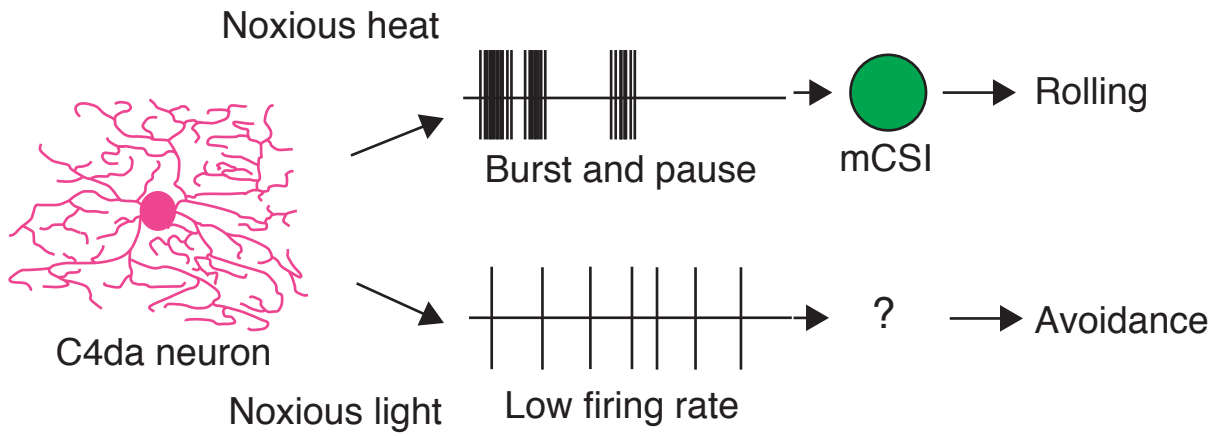

Figure 28. Different neural circuits might exist for nociceptive behaviors

C4da neurons activated by noxious heat exhibit burst and pause firing pattern. This firing pattern might result in the excitation of mCSI and subsequent rolling behavior. By contrast, C4da neurons activated by noxious light exhibit low firing rate. This low firing rate might result in the avoidance behavior.

Conclusion

In this study, using stereotyped escape behavior of *Drosophila* larvae as a model, I identified neural circuitry that evokes the escape behavior, rolling. My main findings are the following:

(1) mCSIs were identified as C4da second order neurons.

- GRASP signals between C4da neurons and mCSIs were detected.
- Ca^{2+} levels in mCSIs were elevated upon the activation of C4da neurons.

(2) mCSIs were necessary and sufficient to evoke rolling behavior upon activation of C4da neurons.

- Activation of mCSIs triggered rolling.
- Silencing of mCSIs reduced the probability of rolling upon activation of C4da neurons.

(3) mCSIs acted in parallel with Basin-Goro pathway.

- Silencing of Goro did not affect the probability of rolling upon activation of mCSIs.
- Silencing of mCSIs did not affect the probability of rolling upon activation of Basins.
- Ca^{2+} levels in Goro was largely unchanged upon activation of mCSIs

(4) mCSIs send output toward motor domains in the VNC, and SNa motor neurons are at least in part functional downstream of mCSIs.

- Axons of mCSIs and dendrites of SNa motor neurons were in close apposition.
- Ca^{2+} levels in SNa motor neurons were elevated following the activation of mCSIs.
- Silencing of SNa motor neurons reduced the probability of rolling upon mCSIs/C4da activation.

These findings are consistent with the hypothesis that there might be (an)other neural circuit(s) that can trigger or facilitate rolling in parallel with Basin-Goro pathway.

Identification of one such circuit, C4da-mCSI-SNa, would help to elucidate how stereotyped rolling behavior is generated.

Acknowledgements

I would like to express my deepest and sincere gratitude to my supervisor, Dr. Kazuo Emoto (The University of Tokyo) for providing the opportunity to study in a splendid environment.

I would like to thank Dr. David Anderson (California Institute of Technology), Dr. Gerald Rubin (Janelia Research Campus), Dr. Iris Salecker (The Francis Crick Institute), Bloomington Stock Center, and Kyoto Stock Center for fly stocks; Dr. Peter Soba (Center for Molecular neurobiology, Hamburg) for communicating unpublished data; Dr. Jay Z Parrish (University of Washington) for critical reading of the paper.

I would like to give thanks to Dr. Hiroyuki Takeda (The University of Tokyo) for encouraging me to dedicate myself to scientific research.

I am truly grateful to the member of Emoto lab (the laboratory of Brain function, Department of Biological Sciences, Graduate School of Science, The university of Tokyo), Dr. Rei Morikawa for analysis of mCSI dendrite patterning (Figure 17) and teaching me the basis of *Drosophila* neurobiology and techniques for neuroscience research, Dr. Eri Hasegawa for data of the SNa motor neuron projection (Figure 22B) and technical advises about motor neurons, Mr. Masato Tsuji for advise about statistical methods, Ms. Emilia Bergoglio for proofreading and other members for critical comments and discussion; Mrs. Mado Miyahara and Mr. Hajime Itoh for technical assistants.

Finally, I am greatly indebted to my family and friends for their heartfelt support and generous affection, without which I could not have accomplished this study. I dedicate my doctoral thesis to them.

References

Adams, CM., Anderson MG., Motto, DG., Price, MP., Johnson, WA., and Welsh, MJ. (1998). Ripped pocket and pickpocket, novel *Drosophila* DEG/ENa subunits expressed in early development and in mechanosensory neurons. J. Cell Biol. 140, 143-152.

Babcock, DT., Landry, C., and Galko, MJ. (2009). Cytokine signaling mediates UV-induced nociceptive sensitization in *Drosophila* larvae. Curr. Biol. 19, 799-806.

Babcock, DT., Shi, S., Jo, J., Shaw, M., Gutstein, HB., and Galko, MJ. (2011). Hedhehog signaling regulates nociceptive sensitization. Curr. Biol. 21, 1525-1533.

Basbaum, AI., and Jessell, T. (2000). The perception of pain. In Principles of Neuroscience, E.R. Kandel, J Schwartz, abd T. Jessell, eds. (New York; Appleton and Lange), pp. 472-491.

Bautista, DM., Siemens, J., Glazer, JM., Tsuruda, PR., Basbaum, AI., Stucky, CL., Jordt, SE., and Julius, D. (2007). The menthol receptor TRPM8 is the principal detector of environmental cold. Nature 448, 204-208.

Bennett, DL., and Woods CG. (2014). Painful and painless channelopathies. THE LANCET Neurology 13, 587-599.

Berni, J., Pulver, SR., Griffith, LC., and Bate, M. (2012). Autonomous circuitry for substrate exploration in freely moving *Drosophila* larvae. Curr. Biol. 22, 1861-1870.

Bodmer, R., Jan, YN. (1987). Morphological differentiation of the embryonic peripheral neurons in *Drosophila.* Roux Arch Dev Biol 196, 69-77.

Boyden, ES., Zhang, F., Bamberg, E., Nagel, G., Deisseroth, K. (2005). Millisecond-timescale, genetically targeted optical control of neural activity. Nat Neurosci 8, 1263-1268.

Brand, AH., and Perrimon, N. (1993). Targeted gene expression as a means of altering cell fates and generating dominant phenotypes. Development 118, 401-415.

Caldwell, JC., Miller, MM., Wing, S., Soll, DR., and Eberl, DF. (2003). Dynamic analysis of larval locomotion in *Drosophila* chordotonal organ mutants. Proc Natl Acad Sci USA 100, 16053-16058.

Caterina, MJ., Schumacher, MA., Tominaga, M., Rosen, TA., Levine, JD., and Julius, D. (1997). The capsaicin receptor: a heat-activated ion channel in the pain pathway. Nature 389, 816-824.

Cheng, LE., Song, W., Looger, LL., Jan, LY., and Jan YN. (2010). The role of the TRP channel NompC in *Drosophila* larval and adult locomotion. Neuron 67, 373-380.

Christiansen, F., Zube, C., Andlauer, TF., Wichmann, C., Fouquet, W., Owald, D., Mertel, S., Leiss, F., Tavosanis, G., Farca Luna, AJ., Fiala, A., and Sigrist, SJ. (2011). Presynapses in Kenyon Cell Dendrites in the Mushroom Body Calyx of *Drosophila*. J. Neurosci. 31, 9696-9707.

Clyne, JD., and Miesenbock, G. (2008). Sex-specific control and tuning of the pattern generator for courtship in *Drosophila*. Cell 133, 354-363.

Cordero-Erausquin, M., Inquimbert, P., Schlichter, R., and Hugel, S. (2016). Neuronal networks and nociceptive processing in the dorsal horn of the spinal cord. Neuroscience 338, 230-247.

Coste, B., Mathur, J., Schmidt, M., Earley, TJ., Ranade, S., Petrus, MJ., Dubin, AE., and Patapoutian, A. (2010). Piezo1 and Piezo2 are essential components of distinct mechanically activated cation channels. Science 330, 55-60.

Dubin, AE., and Patapoutian, A. (2010). Nociceptors: the sensors of the pain pathway. J

Clin Invest 120, 3760-3772.

Emoto, K. (2012). Signaling mechanisms that coordinate the development and maintenance of dendritic fields. Curr. Opin. Neurobiol. 22, 805-811.

Feinberg, EH., Vanhoven, MK., Bendesky, A., Wang, G., Fetter, RD., Shen, K., and Bargmann, CI. (2008). GFP reconstitution across synaptic partners (GRASP) defines cell contacts and synapses in living nervous systems. Neuron 57, 353-363.

Feng, Y., Ueda, A., and Wu, CF. (2004). A modified minimal hemolymph-like solution, HL3.1, for physiological recordings at the neuromuscular junctions of normal and mutant *Drosophila* larvae. J. Neurogenet 18, 377-402.

Garces, A., Bogdanik, L., Thor, S., and Carroll, P. (2006). Expression of *Drosophila* BarH1-H2 homeoproteins in developing dopaminergic cells and segmental nerve a (SNa) motoneurons. Eur. J. Neurosci. 24, 37-44.

Grueber, WB., Jan, LY., and Jan, YN. (2002) Tiling of the *Drosophila* epidermis by multidendritic sensory neurons. Development 129, 2867-2878.

Gruber, WB., Ye, B., Moore, AW., Jan, LY., and Jan, YN. (2003). Dendrites of distinct classes of *Drosophila* sensory neurons show different capacities for homotypic repulsion. Curr. Biol 15, 618-626.

Grueber, WB., Ye, B., Yang, CH., Younger, S., Borden, K., Jan, LY., and Jan, YN. (2007). Projections of *Drosophila* multidendritic neurons in the central nervous system: links with peripheral dendrite morphology. Development 134, 55-64.

Guo, Y., Wang, Y., Wang, Q., and Wang, Z. (2014). The role of PPK26 in *Drosophila* larvae mechanical nociception. Cell Rep. 9, 1183-1190.

Han, C., Wang, D., Soba, P., Zhu, S., Lin, X., Jan, LY., and Jan, YN. (2012). Integrins

regulate repulsion-mediated dendritic pattering of *Drosophila* sensory neurons by restricting dendrites in 2D space. Neuron 73, 64-78.

Honjo, K., Mauthner, SE., Wang, Y., Skene, JH., and Tracey, WD. (2016). Nociceptor-enriched genes required for normal thermal nociception. Cell Rep. 16, 295-303.

Hwang, RY., Zhong, L., Xu, Y., Johnson, T., Zhang, F., Deisseroth, K., and Tracey, WD. (2007). Nociceptive neurons protect *Drosophila* larvae from parasitoid wasp. Curr. Biol. 17, 2105-2116.

Iggo, A., Steedman, WM., and Fleetwood-Walker, S. (1985). Spinal processing: anatomy and physiology of spinal nociceptive mechanisms. Philos. Trans. R. Soc. Lond. B. Biol. Sci. 308, 235-252.

Im, S.H., and Galko, MJ. (2012). Pokes, sunburn, and hot sauce: *Drosophila* as an emerging model for the biology of nociception. Dev. Dyn. 241, 16-26.

Im SH., Takle, K., Babcock, DT., Ma, Z., Xiang, Y., and Galko, MJ. (2015). Tachykinin acts upstream of autocrine Hedgehog signaling during nociceptive sensitization in *Drosophila*. Elife 4, e10735.

Jan, YN., and Jan, LY. (2010). Branching out: mechanisms of dendrite arborization. Nat. Rev. Neurosci. 11, 316-328.

Jenett, A., Rubin, GM., Ngo, TT., Shepherd, D., Murphy, C., Dionne, H., Pfeiffer, BD., Cavallaro, A., Hall, D., Jeter, J., et al. (2012). A GAL4-driver line resource for *Drosophila* neurobiology. Cell Rep. 2, 991-1001.

Kanamori, T., Kanai, MI., Dairyo, Y., Yasunaga, K., Morikawa, KR., and Emoto, K. (2013). Compartmentalized calcium transients trigger dendrite pruning in *Drosophila* sensory neurons. Science 340, 1475-1478.

Kanamori, T., Togashi, K., Koizumi, H, and Emoto, K. (2015). Dendritic remodeling: Lessons from invertebrate model systems. Int. Rev. Mol. Biol. 318, 1-25.

Kanamori, T., Yoshino, J., Yasunaga, K., Dairyo., Y., and Emoto, K. (2015). Local endocytosis triggers dendritic thinning and pruning in *Drosophila* sensory neurons. Nature Communications 12, 6; 6515.

Kim, SE., Coste, B., Chadha, A., Cook, B., and Patapoutian, A. (2012). The role of *Drosophila* Piezo in mechanical nociception. Nature 483, 209-212.

Kohsaka, H., Okusawa, S., Itakura, Y., Fushiki, A., and A, Nose. (2012). Development of larval motor circuits in *Drosophila*. Dev Growth Differ 54, 408-419.

Koike-Kumagai, M., Yasunaga, K., Morikawa, R., Kanamori, T., and Emoto, K. (2009). The target of rapamycin complex 2 controls dendritic tiling of *Drosophila* sensory neurons through the Tricornered kinase signaling pathway. EMBO J. 28, 3879-3892.

Lai, SL., and Lee, T. (2006). Genetic mosaic with dual binary transcriptional systems in *Drosophila*. Nat Neurosci 9, 703-709.

Lin, JY., Knutsen, PM., Muller, A., Kleinfeld, D., and Tsien, RY. (2013). ReaChR: a red-shifted variant of channelrhodopsin enables deep trascranial optogenetic excitation. Nat. Neurosci. 16, 1499-1508.

Loeser, JD., and Treede, RD. (2008). The Kyoto protocol of IASP Basic Pain Terminology. Pain 137, 473-477.

Ma, J., and Ptashne, M. (1987). A new class of yeast transcriptional activators. Cell 51, 113-119.

Macpherson, LJ., Zaharieva, EE., Keamey, PJ., Alpert, MH., Lin, TY., Turan, Z., Lee, CH., and Gallio, M. (2015). Dynamic labelling of neural connections in multiple colours

by trans-synaptic fluorescence complementation. Nat. Commun 6, 10024.

Mauthner, SE., Hwang, RY., Lewis, AH., Xiao, Q., Tsubouchi, A., Wang, Y., Honjo, K., Skene, JH., Grandl, J., and Tracey, WD. (2014). Balboa binds to pickpocket in vivo and is required for mechanical nociception in *Drosophila* larvae. Curr. Biol. 24, 2920-2925.

Morikawa, RK., Kanamori, T., Yasunaga, K., and Emoto, K. (2011). Different levels of the tripartile motif protein, Anomalies in sensory axon patterning (Asap), regulate distinct axonal projections of *Drosophila* sensory neurons. Proc Natl Acad. Sci USA 108, 19389-19394.

Nagel, G., Szellas, T., Huhn, W., Kateriya, S., Adeishvili, N., Berthold, P., Ollig, D., Hegemann, P., and Bamberg, E. (2003). Channelrhodpsin-2, a directly light-gated cation selective membrane channel. Proc Natl Acad Sci USA 100, 13940-13945.

Neely, GG., Keene, AC., Duchek, P., Chang, EC., Wang, QP., Aksoy, YA., Rosenzweig, M., Costigan, M., Woolf, CJ., Gamty, PA., and Penninger, JM. (2011). TrpA1 regulates thermal nociception in *Drosophila*. PLoS One 6, e24343.

Nicolaï, LJ., Ramaekers, A., Raemaekers, T., Drozdzecki, A., Mauss, AS., Yan, J., Landgraf, M., Annaert, W., and Hassan, BA. (2010). Genetically encoded dendritic marker sheds light on neuronal connectivity in *Drosophila*. Proc Natl Acad Sci USA 107, 20553-20558.

Ohyama, T., Schneider-Mizell, CM., Fetter, RD., Aleman, JV., Franconvill, R., Rivera-Alba, M., Mensh, BD., Branson, KM., Simpson, JH., Truman, JW., Cardona, A., and Zlatic, M. (2015). A multilevel multimodal circuit enhances action selection in *Drosophila*. Nature 520, 633-639.

Pfeiffer, BD., Ngo, TT., Hibbard, KL., Murphy, C., Jenett, A., Truman, JW., and Rubin,

GM. (2010). Refinement of tools for targeted gene expression in *Drosophila*. Genetics 186, 735-755.

Picao-Osorio, J., Johnston, J., Landgraf, M., Bemi, J., and Alonso, CR. (2015). MicroRNA-encoded behavior in *Drosophila*. Science 350, 815-820.

Potter, CJ., Tasic, B., Russeler, EV., Liand, L., and Luo, L. (2010). The Q system: a repressible binary system for transgene expression, lineage tracing, and mosaic analysis. Cell 141, 536-548.

Robertson, JL., Tsubouchi, A., and Tracey, WD. (2013). Larval defense against attack from parasitoid wasps requires nociceptive neurons. PLoS One 8, e78704.

Sato, M., Kojima, T., Michiue, T., and Saigo, K. (1999). Bar homeobox genes are latitudinal prepattern genes in the developing *Drosophila* notum whose expression is regulated by the concerted functions of decapentaplegic and wingless. Development 126, 1457-1466.

Sweeney, ST., Broadie, K., Keane, J., Niemann, H., and O'Kane, CJ. (1995). Targeted expression of tetanus toxin light chain in *Drosophila* specifically eliminates synaptic transmission and causes behavioral defects. Neuron 14, 341-351.

Terada, S., Matsubara, D., Onodera, K., Matsuzaki, M., Uemura, T., and Usui, T. (2016). Neuronal processing of noxious thermal stimuli mediated by dendritic Ca^{2+} influx in *Drosophila* somatosensory neurons. Elife 5, e12959.

Tracey, WD., Wilson, RI., Laurent, G., and Benzer, S. (2003). painless, a *Drosophila* gene essential for nociception. Cell 113, 261-273.

Tsubouchi, A., Caldwell, JC., and Tracey, WD. (2012). Dendritic filopodia, Ripped Pocket, NOMPC, and NMDARs contribute to the sense of touch in *Drosophila* larvae.

Curr. biol 22, 2124-2134.

Venken, KJ., Simpson, J.H., and Bellen, HJ. (2011). Genetic manipulation of genes and cells in the nervous system of the fruit fly. Neuron 72, 202-230.

Walters, ET. (1994). Injury-related behavior and neuronal plasticity: an evolutionary perspective on sensitization, hyperalgesia, and analgesia. Int Rev Neurobiol 36, 325-427.

Walters, ET., and Moroz, LL. (2009). Molluscan memory of injury: evolutionary insights into chronic pain and neurological disorders. Brain Behav Evol 74, 206-218.

Wong, AM., Wang, JW., Axel, R. (2002). Spatial representation of the glomerular map in the *Drosophila* protocerebrum. Cell 19, 229-241.

Woolf, CJ., and Wakters, ET. (1991). Common patterns of plasticity contributing to nociceptive sensitization in mammals and Aplysia. Trends Neurosci 14, 74-78.

Xiang, Y., Yuan, Q., Vogt, N., Looger, LL., Jan LY., and Jan YN. (2010). Light-avoidance-mediating photoreceptors tile the *Drosophila* larval body wall. Nature 468, 921-926.

Yan, Z., Zhang, W., He, Y., Gorczyca, D., Xiang, Y., Cheng, LE., Meltzer, S., Jan, LY., and Jan, YN. (2013). *Drosophila* NOMPC is a mechanotransduction channel subunit for gentle-touch sensation. Nature 493, 221-225.

Yang, L., Li, R., Kaneko, T., Takle, K., Morikawa, RK., Essex, L., Wang, X., Zhou, J., Emoto, K., Xiang, Y., and Ye, B. (2014). Trim9 regulates activity-dependent fine-scale topography in *Drosophila*. Curr. Biol. 24, 1024-1030.

Yasunaga, K., Kanamori, T., Morikawa, R., and Emoto, K. (2010). Dendrite reshaping of adult *Drosophila* sensory neurons requires matrix metalloproteinase- mediated modification of the basement membranes. Dev. Cell 18: 621-632 (2010).

Zhang, W., Yan, Z., Jan, LY., and Jan, YN. (2013). Sound response mediated by the TRP channels NOMPC, NANCHUNG, and INACTIVE in chordotonal organs of *Drosophila* larvae. Proc Natl Acad Sci USA 110, 13612-13617.

Zhong, L., Hwang, RY., and Tracey, WD. (2010). Pickpocket is a DEG/ENaC protein required for mechanical nociception in *Drosophila* larvae. Curr Biol 20, 429-434.